AUSTRALIAN NATIONAL ANTARCTIC RESEARCH EXPEDITIONS

A N A R E

R E S E A R C H

N O T E S

14

The Variation of Southern Hemisphere Atmospheric Vorticity Around Interplanetary Magnetic Field Sector Crossings

Gary Burns

ANTARCTIC DIVISION
DEPARTMENT OF SCIENCE AND TECHNOLOGY

ANARE RESEARCH NOTES (ISSN 0729-6533)

This series complements ANARE Reports and incorporates the functions of the now discontinued series of Technical Notes and Antarctic Division Technical Memoranda. The series will allow rapid publication in a wide range of disciplines. Copies of ANARE Research Notes are available from the Antarctic Division.

Any person who has participated in Australian National Antarctic Research Expeditions is invited to publish through this series. Before submitting manuscripts authors should obtain a style guide from:

The Publications Office
Antarctic Division
Channel Highway
Kingston
Tasmania 7150
Australia.

Published December 1983
ISBN: 0 642 87733 5

CONTENTS

FIGURES

TABLES

THE VARIATION OF SOUTHERN HEMISPHERE ATMOSPHERIC VORTICITY AROUND INTERPLANETARY MAGNETIC FIELD SECTOR CROSSINGS

by

Gary Burns

Antarctic Division,
Department of Science and Technology,
Hobart, Tasmania, Australia

ABSTRACT

The variation of a Southern Hemisphere absolute vorticity area index about solar sector boundary crossings is examined by the superposed epoch method. It is concluded that the Southern Hemisphere results do not confirm the winter decrease in vorticity near sector crossings found by researchers using Northern Hemisphere data. There is, however, limited indication that the following southern hemisphere effects may exist:

(a) A vorticity decrease in the summer months showing a shape similarity to the Northern Hemisphere winter response.

(b) A winter peak in vorticity on the boundary crossing date for the Australian quadrant of the Southern Hemisphere.

1. INTRODUCTION

Wilcox et al. (1973, 1974) reported that the average area of high absolute atmospheric vorticity in the Northern Hemisphere decreases near the times when the Interplanetary Magnetic Field (IMF) sector boundaries are carried past the earth by the solar wind.

The solar magnetic sector structure extends radially out from the sun carried by the solar wind. From the earth the IMF can be divided into sectors of opposite polarity. The division is made on the basis of whether the IMF is directed predominantly towards or away from the Sun. Normally four boundaries, at approximately equal time intervals, sweep past the earth during each solar rotation (approximately 27 days).

Wilcox et al. (1973, 1974) used 300 mb geopotential height maps for 0000 and 1200 GMT each day to compute vorticity maps, at the 300 mb level, for the area poleward of geographic latitude 20°N. A discriminator of 2.0 x 10-4 sec-1 was applied to the vorticity map and the area in which the vorticity exceeded this value was recorded. The discriminator was then set at 2.4 x 10-4 sec-1 and the area in which the vorticity exceeded this value was added to the previously computed area. In some later investigations a single discriminator was used. The Vorticity Area Index (VAI) so calculated had a diurnal variation and in order to remove this the VAI was smoothed using the formula

$$V_i' = 0.25*V_{i-1} + 0.5* V_i + 0.25*V_{i+1}$$

where V_{i-1}, V_i, V_{i+1} refer to successive values at 12 hour intervals and V_i' is the resultant smoothed value.

Sector crossings of the IMF were chosen from spacecraft observations. To be chosen as a sector crossing date the boundary crossing needed to be preceded by a predominant polarity of the IMF for at least 4 days. The dates so chosen were used as key dates for a superposed epoch analysis of the vorticity area index.

Wilcox et al. (1974), using a VAI calculated using the 2.0 x 10-4 sec-1 discriminator only, found that the observed dip persisted at the 200 mb, 300 mb, 500 mb, 700 mb and 850 mb levels of the Troposphere. The effect was most prominent at 300 mb. They also carried out an analysis in which the VAI at each height was kept approximately equal to 40 x 105 km2 by altering the discriminator used at each height. Similar results were obtained. The effect was found to be not prominent in the Stratosphere at the 100 mb, 50 mb, 30 mb and 10 mb levels although a peak in VAI 4 days after the boundary crossing at the 100 mb level was claimed as "probably significant".

By splitting the 300 mb data into longitudinal intervals of 60° each the investigators found that all six resulting curves, noisy though they were, exhibited a minimum near the passing of a sector boundary. They concluded that the global effect at 300 mb did not come from one or two prominent longitudinal intervals.

Wilcox et al. (1975) extended the earlier work. They increased the time interval to from 1963 to 1973 and the number of boundary

crossings from 54 to 131. This extension of key dates was made by using information on the polarity of the IMF inferred from polar geomagnetic observations as well as satellite magnetometer data which was the only data previously used. (This technique is reviewed by Wilcox, 1972). Wilcox et al. (1975) used a 500 mb VAI obtained using a discriminator setting of 2.0×10^{-4} sec^{-1}. The reason given for changing to the 500 mb data was the greater homogeneity of the 500 mb observations. They filtered the VAI to remove variations corresponding to periods greater than 13 days and less than 3 days. They considered 6 two-month periods of key dates and the results showed a 10% decrease in vorticity at day one only in the winter months.

Wilcox et al. (1976) further tested the new data by calculating the winter curve resulting from using the new key dates only, and separately, the new key dates obtained only from the satellite observations. The original effect of a 10% decrease in absolute vorticity one day after the boundary crossing (day one) was found to persist.

2. NORTHERN HEMISPHERE ERROR ANALYSIS

Wilcox et al. (1974) calculated a 'probable error' associated with the value of the VAI at day one. They did not wish to include long-term variations, i.e. periods longer than the 12 day variation around the sector boundary crossing, in the calculation of the standard error. They therefore computed the average value of the VAI during the interval ± 6 days from the boundary crossing date for each boundary crossing, A_j, as follows. Let each vorticity area index be designated by a double indexed number V_{ij} where i runs from 1 to 25 (the number of half-day units in the interval used) and j runs from 1 to 54 (the number of boundary crossings in the interval considered). Then

$$A_j = \frac{1}{25} \sum_{i=1}^{25} V_{ij}$$

From this value, A_j, they subtracted the grand average of the vorticity area index during all days in the intervals ± 6 days from the 54 boundary crossings considered, A.

$$A = \frac{1}{54} \sum_{j=1}^{54} A_j$$

$$A_j' = A_j - A$$

They then subtracted the resulting value, A_j', from the value of the vorticity on day one, V_{1j}, for the respective boundary crossing

$$V_{1j}' = V_{1j} - A_j'$$

Wilcox et al. (1974) then considered the range within which 65% of these V_{ij}' values occurred and divided this by $\sqrt{53}$, to obtain an estimate of the probable error.

Hines and Halevy (1977) using the same data as Wilcox et al. (1973, 1974) calculated the most probable error for all half-days within the ± 6 day interval of the boundary crossings. They calculated this probable error as the root-mean-square of the $(V_{ij} - A_j')$ values, divided by $\sqrt{n-1}$, where n is the number of boundary crossings. Their method reduces to that of Wilcox et al. (1974) if the distribution of the $(V_{ij} - A_j')$ values is a normal distribution.

Hines and Halevy (1977) obtained an estimated probable error of $\pm 1.97 \times 10^5$ km^2 for day one after the boundary crossings compared with Wilcox et al. (1974) who had obtained $\pm 1.6 \times 10^5$ km^2. For all but one of the other half-days, the estimated error was greater than $\pm 1.97 \times 10^5$ km^2. The full range of errors calculated by this method ranged from $\pm 1.90 \times 10^5$ km^2 to $\pm 2.80 \times 10^5$ km^2 with a mean of $\pm 2.31 \times 10^5$ km^2.

Hines and Halevy (1977) pointed out that as the amplitude of the signal presented by Wilcox et al. (1973) is approximately 10×10^5 km^2 their result would still remain an impressive test of the statistical significance of the deviation that constitutes the presumed signal, provided that the noise being averaged out was white noise (i.e. had no internal correlations). The method of dividing the r.m.s. value by $\sqrt{n-1}$, where n is the number of samples, is a method strictly valid only for a random sampling of white noise.

Meteorological data is, however, correlated with itself over periods of several days and the implication of the error bars calculated is thus in doubt. Wilcox et al. (1973, 1974) compounded these problems of internal correlations by averaging to remove long-term variations within their data. This has been noted in the literature by Shapiro (1976) who says, "In attempting to eliminate long-term seasonal variations from the calculations of the standard error Wilcox et al. (1974) also removed a significant part of some shorter period variations. More than 30% of the variation contributed by periods of 2-3 weeks and about 60% of the variation due to 3-4 week periods are eliminated ... thus ... the estimate of the standard error is too small and probably significantly so."

The only way of testing the extent to which the curve presented by Wilcox et al. (1973, 1974) varies from a random curve is by generating random curves from the same data and comparing them in an analytical way with the alleged signal. This was the approach used by Hines and Halevy (1977).

Hines and Halevy (1977) introduced a parameter which they called the excursion, x. It is defined as the difference between the maximum and minimum values of the VAI found in a 12 day interval. The excursion of the original curve derived by Wilcox et al. (1973) (Figure 2a) is 12.43 in units of 10^5 km2. Hines and Halevy (1977) calculated the excursions of each of 200 curves consisting of a superposed epoch analysis of 54 random key dates, 54 being the number of solar sector boundary crossings used in the original analysis. The only criterion for selection of these random key days was that no key day could be within 4 days of one already chosen. This matches a prohibition on the selection of solar sector boundaries used by Wilcox et al. (1973, 1974) and is also a general condition of the structure of the interplanetary magnetic field.

The random curves had an ensemble average excursion of 7.57 ± 1.98 (r.m.s. value) in units of 10^5 km^2. The excursion of Wilcox et al. (1973) curve therefore lies at 2.45σ above the mean of these random excursions. For a normal distribution of excursion values this would occur as a random chance in less than 2% of cases. Of the 200 curves generated by Hines and Halevy (1977), 4 had excursions greater than the original curve and 2 had excursions nearly as great. They therefore concluded that the original curve would have been produced by pure chance with at most a 2 to 3% probability.

This probability cannot be taken as conclusive evidence that the effect is real. This method of analysis cannot take into account any 'tuning-up' of the data which may have resulted from the authors searching for a 'best case'. In that situation this approach simply measures how successful they have been!

An example of a possible 'tuning-up' of the data by Wilcox et al. (1973, 1974) was found by Shapiro (1976). In their superposed epoch analysis Wilcox et al. (1973, 1974) used solar sector crossings which occurred in the Northern Hemisphere winter 5 months of November to March inclusive. Shapiro (1976) found that the inclusion of the October data in the analysis reduced the significance of the dip found in the other 5 months. There is no a priori reason for excluding the October sector crossing dates from the analysis and their exclusion on the basis that they do not enhance the effect provides a method of artificially enhancing the statistical significance. This is not an invalid method of searching for a relationship but the validity of a

relationship so found can only be fully tested using new and independent data. This point was made by Hines and Halevy (1977) when they stated, "Meaningful reality of a claimed correlation cannot be tested adequately by means of the original correlation itself."

The extended analysis of Wilcox et al. (1975, 1976) provided the new data for further testing of the reality of the vorticity response. The persistence of the 10% decrease in vorticity on day one in the new data, although it is 500 mb filtered data, provided a significant test of the validity of the effect and justified the search for a similar or related result in the Southern Hemisphere.

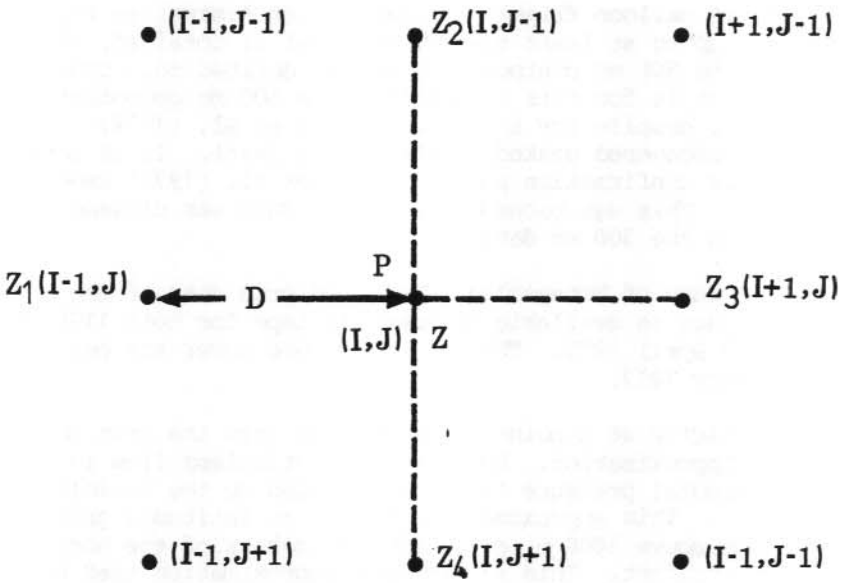

Figure 1. The Australian Bureau of Meteorology grid system.

3. THE SOUTHERN HEMISPHERE METEOROLOGICAL DATA

The meteorological data used in this analysis was derived in the following manner. From balloon flights, direct measurements are made of the heights of the various pressure levels. There are approximately 50 balloon flight stations within Australia. The results of similar flights in South America, South Africa, New Zealand and on the Antarctic mainland are also obtained. Satellite photographs, where these are available, are used to give an indication of the circulation pattern over the vast expanses of ocean in the Southern Hemisphere. By measuring cloud cell sizes it is possible to obtain an estimate of the height of the 500 mb level from these photographs. With these values at his disposal a forecaster draws the contour heights for the various pressure levels for the entire Southern Hemisphere. This drawing is then digitized in grid form and stored on magnetic tape.

Similar methods are used in the Northern Hemisphere to calculate the geopotential height maps that were used by Wilcox et al. (1973, 1974, 1975, 1976) as the basis for their calculation of absolute vorticity. Because of the larger number of measuring stations and the smaller percentage of ocean area in the Northern Hemisphere it is apparent that the data used by Wilcox et al. will be the more accurate. The freehand drawing that goes into the maps made by the forecaster makes it difficult to estimate the extent to which the Southern Hemisphere data is inferior to the Northern Hemisphere data. It is important to note, however, that this difference does exist.

One requirement of balloon flight measurements at Australian stations is that unless a reading up to at least the 500 mb level is obtained, the flight is repeated. Thus the 500 mb contours are better defined than those of any lower pressure level. It is for this reason that the 500 mb geopotential height was used in this work, despite the fact that Wilcox et al. (1974) reported that the effect they had discovered peaked at the 300 mb level. It is interesting to note that in their confirmation paper, Wilcox et al. (1976) used 500 mb vorticity values. This was becasue the 500 mb data was claimed to be more 'homogeneous' than the 300 mb data.

The Australian Bureau of Meteorology digitised grid data of the 500 mb geopotential heights is available on magnetic tape for both 1100 GMT and 2300 GMT dating from 9 April 1973. The data used here cover the period from 9 April 1973 to 28 February 1977.

The absolute vorticity at a point is calculated from the grid point data using the geostrophic approximation. Horizontal frictionless flow in which the atmospheric horizontal pressure force is balanced by the Coriolis Force is said to be geostrophic. This approximation is good at latitudes greater than 20° and at elevations above 1000 m, provided the isobars of the horizontal level maps are nearly straight. This is the same approximation used by Shapiro (1976) in his check of the results of Wilcox et al. Wilcox et al. (1973, 1974) do not state what approximations, if any, they used to calculate the vorticity. They state that it was computed from geopotential height data and is valid north of 20°N. The geostrophic approximation is the easiest way to do this within the limitations stated.

Using the nomenclature of Figure 1, the absolute vorticity at point P is given by

$$\nu = \frac{4g}{fD^2}\left(\frac{Z_1 + Z_2 + Z_3 + Z_4}{4} - Z\right) + f$$

where

$f = 2\Omega \sin\phi$ is the coriolis parameter; Ω is the angular velocity of the earth, ϕ the latitude of the point in question; g is the gravitational acceleration, D is the average separation of the grid points at latitude ϕ

Z is the geopotential height at the point in question

Z_1, Z_2, Z_3 and Z_4 are the geopotential heights at the surrounding grid points as indicated in Figure 1.

With each of the 845 grid points below 20°S was associated an area D^2. The vorticity value at each of the grid points poleward of 20°S was then compared with a threshold value. If it were greater than this threshold value then the area associated with that grid point was added to a cumulative area total. When all the grid points have been so examined, the resultant area total is the unsmoothed vorticity area index associated with that date, time and that particular vorticity threshold.

The absolute vorticity thresholds used by Wilcox et al. (1973, 1974) are not directly compatible with the Southern Hemisphere dates. By summing the area with absolute vorticity greater than 2.0×10^{-4} sec^{-1} with that for which the absolute vorticity was greater than 2.4×10^{-4} sec^{-1} Wilcox et al. (1973) obtained a vorticity area index of approximately 115×10^5 km^2. Since 15% of the total index resulted from the descriminator 2.4×10^{-4} sec^{-1} (Wilcox et al. 1974) it was decided to use an area of 10^7 km^2 as a basis for deciding the threshold to be employed for the Southern Hemisphere analysis.

The separation of the grid points used in this present analysis is approximately 500 km. Thus each grid point has associated with it an area of about 2.5×10^5 km^2. Thus 40 grid points make up the area total of 10^7 km^2. The 10% reduction found by Wilcox et al. would result from a variation of only 4 grid points, a variation which may quite easily occur by chance. It was considered sensible to also investigate vorticity area indices with a higher value where, if the effect were present in a similar magnitude, the variation may not be so readily obtained by random fluctuations. It was decided to use 10 different vorticity thresholds. The threshold giving a vorticity area index of 10^7 km^2 provided a value close to the upper limit of the values of the thresholds used. Table 1 contains a list of the Southern Hemisphere vorticity thresholds used and the average area associated with each threshold for the winter months. This area ranges from 0.45×10^7 km^2 to 6.92×10^7 km^2, or from 3 to 40% of the area poleward of 20°S.

The twice daily unsmoothed vorticity area indices so obtained were averaged using the formula

$$V_i' = 0.25 \times V_{i-1} + 0.5 \times V_i + 0.25 \times V_{i+1}$$

which has been described previously. The purpose of this averaging is to remove a diurnal variation which persists, despite the index being a summation over all longitudes, because of the domination of a high vorticity area to the east of the Andes.

4. SECTOR BOUNDARY CROSSINGS

The dates of the solar sector boundary crossings used in this analysis were obtained from Dr L Svalgaard by private communication. The information contained the nearest 0000 GMT date at which the boundary crossing occurred and the polarity change of the crossing.

Svalgaard inferred the polarity of the interplanetary magnetic field from polar geomagnetic observations. He used a method developed by himself (Svalgaard 1968, 1972) and discovered independently by Mansurov (1969). Comparing the results obtained using this method with results obtained with measurements of the IMF by satellite, correspondence is found in approximately 85% of cases examined. Wilcox and Colburn (1972) points out that space-craft observations of the IMF are in themselves something of an abstraction. There are a few days when the polarity of the IMF, as inferred by satellite magnetometers, is indeterminate or ambiguous.

By using key dates determined from ground based geomagnetic observations the analysis is open to the criticism of Hines (1973). He pointed out that magnetic fluctuations can be induced by at least two distinct classes of mechanism. The first is solar plasma outflow. The second is associated with fluctuating winds in the ionospheric dynamo region. The strongest observed magnetic fluctuations are associated with solar plasma mechanisms but the weaker fluctuations, caused by irregular winds, might contribute the component of fluctuation that is correlated with lower atmosphere behaviour. The criticism suggests that it may be the atmosphere that is influencing the polar magnetic observations and in turn the selection of the key dates.

The defence of this method of key date determination is based on the results of Wilcox et al. (1974). They found that analyses using key dates based solely on satellite data, and key dates that included Svalgaard's inferred polarities, produced similar results.

5. ANALYSIS

A method of analysis similar to that of Wilcox et al. (1973, 1974) was used on the Southern Hemisphere data. Using the solar sector boundary crossing dates as key dates a superposed epoch analysis was carried out on all the half-day smoothed vorticity area indices within ± 6 days of the key date. Thus all the values in the chosen interval that were 6 days prior to a boundary crossing were averaged. Similar averaging was done for all half-days up to 6 days after the crossing. This can only be done for those boundary crossing dates for which there are no data gaps within the ± 6 day window. This analysis is referred to as the 'averaged VAI' analysis.

With each averaged half-day value is associated an error bar similar to that calculated by Wilcox et al. (1974) for day one of the superposed epoch analysis. The error is estimated in the following manner. Let each vorticity area index value be designated by a double indexed number V_{ij} where i runs from 1 to 25 (the number of half-day units in the interval used) and j runs from 1 to n (the number of boundary crossings in the interval considered). The following terms are then defined

$$A_j = \frac{1}{25} \sum_{i=1}^{25} V_{ij}$$

$$\overline{X}_i = \frac{1}{n} \sum_{j=1}^{n} V_{ij}$$

$$A = \frac{1}{n} \sum_{j=1}^{n} A_j$$

$$A_j' = A_j - A$$

$$V_{ij}' = V_{ij} - A_j'$$

The net effect has been to form n sets of numbers with the same mean value, A. This is done so that any seasonal effect in the vorticity area index is eliminated from an estimation of the error. σ_i is then defined as the standard deviation of the V_{ij}' for fixed i.

$$\sigma_i = \sqrt{\sum_{j=1}^{n} (V_{ij} - \overline{X}_i)^2} \; / \sqrt{n}$$

The error estimated for each half-day unit, i, is then given by

$$\varepsilon_i = \sigma_i \; / \sqrt{n-1}$$

This error bar calculation reduces to that of Wilcox et al. (1973) if the distribution of the individual half-day values around the average value is a normal distribution.

The meteorological grid data used in this analysis is not complete. The data values for some of the dates are not available. When one of these 'no-data' dates falls within the superposed epoch window, ± 6 days from the key date, of a solar sector boundary crossing, then that crossing cannot be used in an analysis of the form outlined in the previous section. This is because an

average of the remaining half-day values may yield an effect due to the seasonal variation of the VAI and not directly due to the boundary crossing.

In order to make use of all the data that were available a second analysis procedure was devised. The differences between consecutive 12 hourly observations of the VAI were calculated for all intervals within the data window for which this was possible. All the values available for any particular interval within the 12 day window were then averaged, and from this a curve of the response of the VAI to the solar sector boundary crossing was constructed. This is referred to as the 'twelve hourly variation' data.

An estimation of the error associated with this anslysis was made by dividing the standard deviation of the difference values of the particular interval by the square root of the number of times that interval occurred less one.

As explained previously, this error calculation is a significant under-estimation of the true errors associated with this analysis. It does, however, provide an easy method by which the results of this analysis may be compared wth those of Wilcox et al. (1973, 1974).

An error analysis using random key dates, as devised by Hines and Halevy (1977), was used to give a realistic measure of the deviation of the resultant curves from a random response. In general 50 random sets of key dates were chosen to generate superposed epoch curves. These random key dates had the condition imposed that no key date could be within 4 days of a key date already chosen. This complies with a general condition of the IMF sector crossings. By comparing the mean and the r.m.s. standard deviation of the random curve excursion values an analytical means of measuring the strength of a supposed signal is obtained. The parameter

$$\rho = \frac{x - \bar{x}}{\sigma}$$

is defined, where x is the excursion of the IMF sector crossing key date curve, $\bar{x}$ is the mean excursion of the random key curve and σ is the r.m.s. deviation of the excursions of the random key date curves. Assuming a normal distribution of excursion values around the mean, a value of ρ greater than 2 implies a less than 5% probability that the IMF key date curve has been generated by chance.

6. RESULTS

The Southern Hemisphere data were divided into winter and summer groups. Wilcox et al. (1973), in their analysis, used the 5 Northern Hemisphere winter months of November to March inclusive. The inclusion of the October data was shown by Shapiro (1976) to reduce the significance of the vorticity dip near the crossing dates. In order to avoid this possibility, the data blocks chosen were the 4 winter months of May to August inclusive and the 4 summer months November to February inclusive.

Figures 8 to 11 show resultant superposed epoch curves for the 10 vorticity thresholds for both 'averaged VAI' and 'twelve hourly variation' summer and winter analyses. The results of the respective random key date excursion analyses are shown in Tables 1 to 4.

No significant deviation from a straight line response was found in any of the curves (i.e. no excursion value was greater than two r.m.s. deviations from the mean of the excursions of the random curves). However, for the low vorticity thresholds of 1.16×10^{-4} sec^{-1} and 1.24×10^{-4} sec^{-1} in the summer 4 months averaged VAI data (42 boundary crossings), a shape similarity with the Northern Hemisphere, Wilcox et al. (1973), curve is apparent. These low vorticity thresholds have associated areas of approximately 6.0×10^7 km^2 and 5.0×10^7 km^2 respectively. The 1.16×10^{-4} sec^{-1} threshold curve shows a strong inverse relationship to the average variation of the K_p index around boundary crossing dates published by Wilcox and Colburn (1972). Figure 2 shows the original Northern Hemisphere 300 mb superposed epoch curve, the two similar Southern Hemisphere summer curves, and the average K_p variation around boundary crossing dates.

The notable feature of the Northern Hemisphere curve (Figure 2a) is the minimum 1 day after the boundary crossing date. Both Southern Hemisphere curves show this effect. In order to quantitatively test the significance of this dip, the excursion for ± 1 day, as opposed to ± 6 days, from the boundary was compared with the average and r.m.s. deviation of the excursion found over this period for 100 random curves. The results of this comprison are shown in Table 5.

Of the randomly generated curves 6 had ± 1 day excursions greater than that of the 1.16×10^{-4} sec^{-1} threshold curve while 15 had excursions greater than the 1.24×10^{-4} sec^{-1} threshold curve. These numbers are smaller than the $\rho = + 1.75$ and $\rho = + 1.15\sigma$ limits would indicate due to a skewing in the distribution of the excursion values. A graph of the distribution for the ± 1 day excursion values of the 1.16×10^{-4} sec^{-1} threshold random curves is shown in Figure 3. It can thus be stated that there is a 6% chance that a curve with a variation within ± 1 day of the key dates greater than or equal to the IMF crossing dates curve would be randomly generated from the VAI data.

The apparent inverted similarity of the K_p variation curve and the VAI for a threshold of 1.16×10^{-4} sec^{-1} summer 4 months curve (Figure 2) was investigated in the following way. From the summer 4 months data 50 random curves were generated. The K_p curve was shifted so that its mean equalled the mean of the random curve with which it was being compared. Then it was stretched so that the standard deviation of the 17 half-day points (± 4 days from the IMF crossing date) about this mean equalled that of the random curve. The Kp curve was inverted about the mean and then the dissimilarity, d, of the

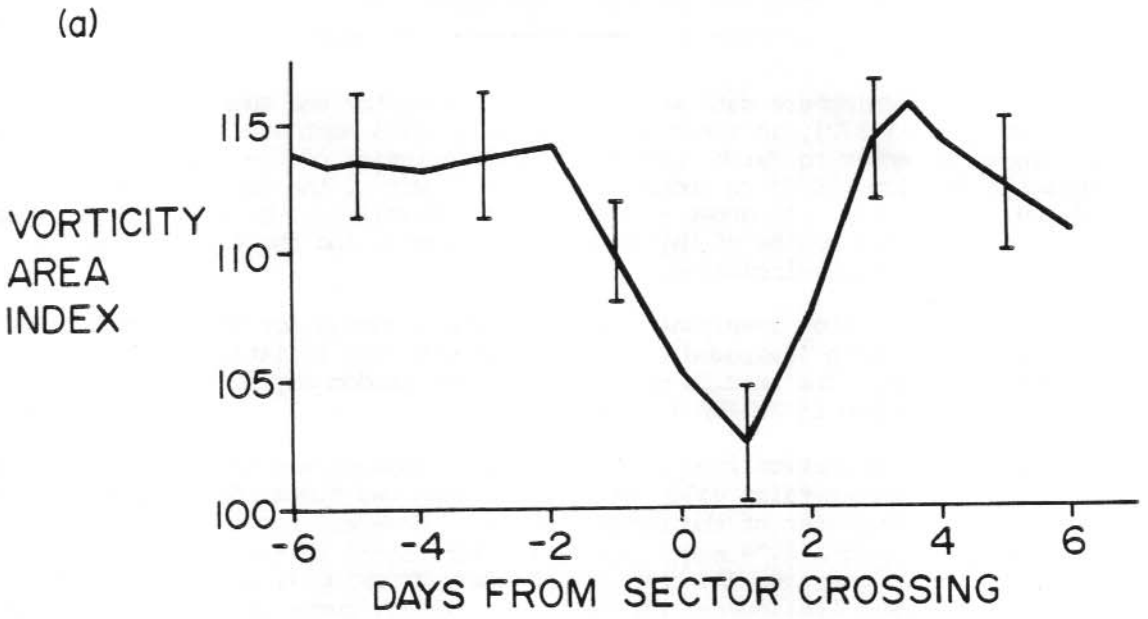

Figure 2. *(a) The original Northern Hemisphere 300 mb, 2.0 x 10^{-4} sec^{-1} plus 2.4 x 10^{-4} sec^{-1} threshold curve (Hines and Halevy, 1977).*

(b) The 1.24 x 10^{-4} sec^{-1} threshold average VAI data curve for the four summer months, in the Southern Hemisphere.

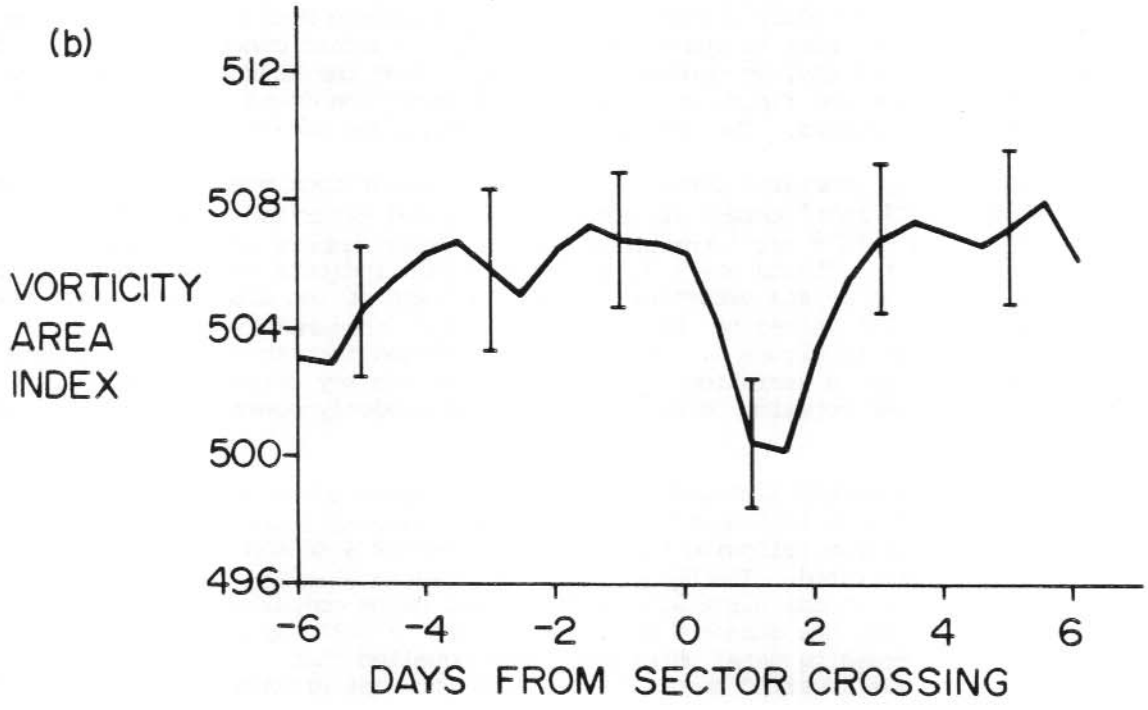

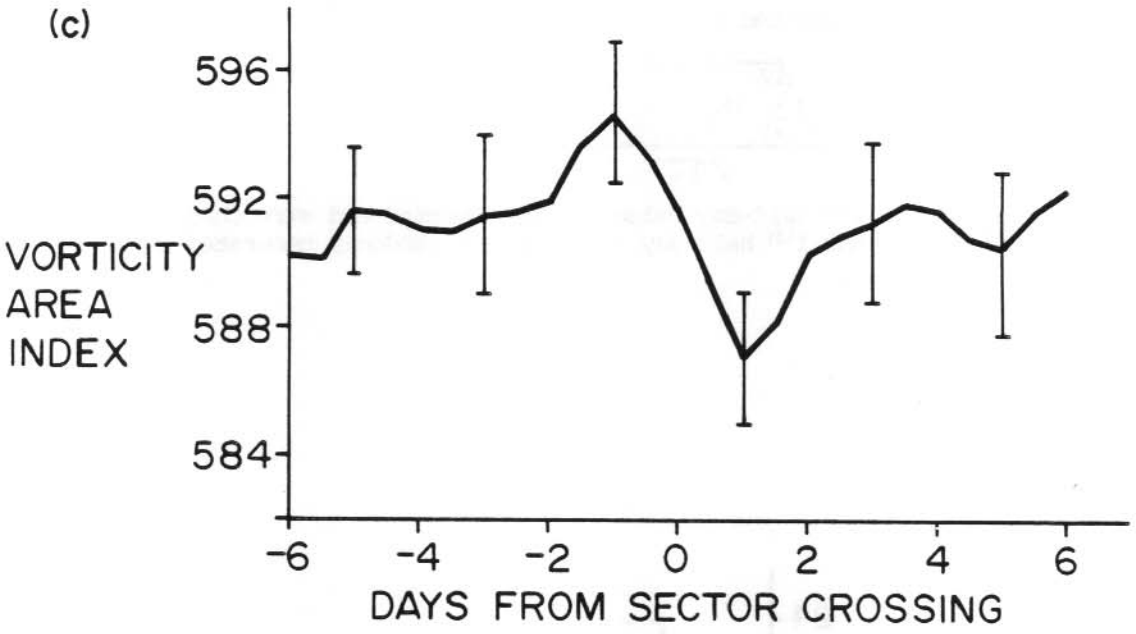

(c) As for (b) but for the 1.16 x 10^{-4} sec^{-1} threshold.

(d) The average variation of the K_p index around the IMF boundary crossing dates (from Wilcox and Colburn, 1972).

two curves was calculated from the expression

$$d = \frac{\sqrt{\sum_{i=1}^{17} (K_i - R_i)^2}}{\sqrt{16}}$$

where K_i is the i^{th} half-day value of the inverted and stretched K_p curve and R_i is the i^{th} half-day value of the randomly generated curve.

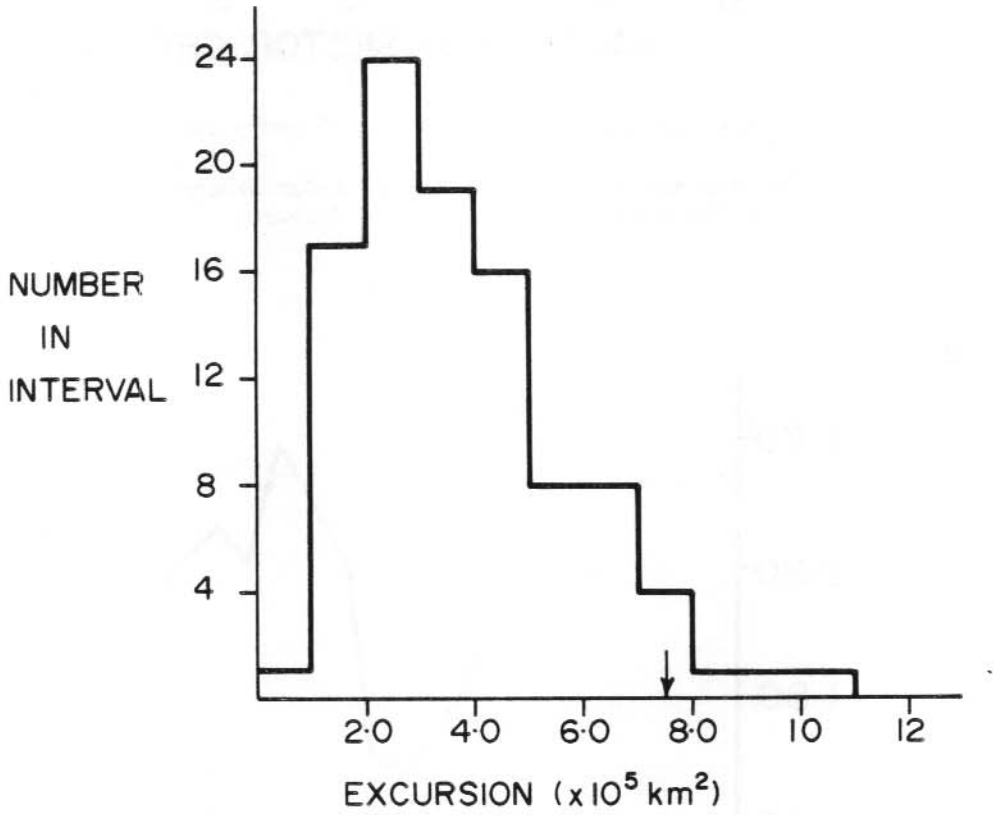

Figure 3. Distribution of the 'excursion' values of 100 random sets of key date curves. The excursion of the 1.16 x 10^{-4} sec^{-1} threshold IMF data curve is arrowed.

The mean and r.m.s. deviation of the dissimilarities for the 50 random curves were 0.282 x 10^6 km^2 and 0.83 x 10^5 km^2 respectively, while the dissimilarity factor for the IMF data curve was 0.88 x 10^5 km^2. This is 2.34 below the mean. None of the 50 random curves came closer to approximating the inverted K_p variation curve than the IMF data. The smallest random dissimilarity value was 0.130 x 10^6 km^2. Figure 4 shows the distribution of the dissimilarity values. Thus the chance of randomly generating a curve that so closely resembles the inverted K_p curve is less than 3%.

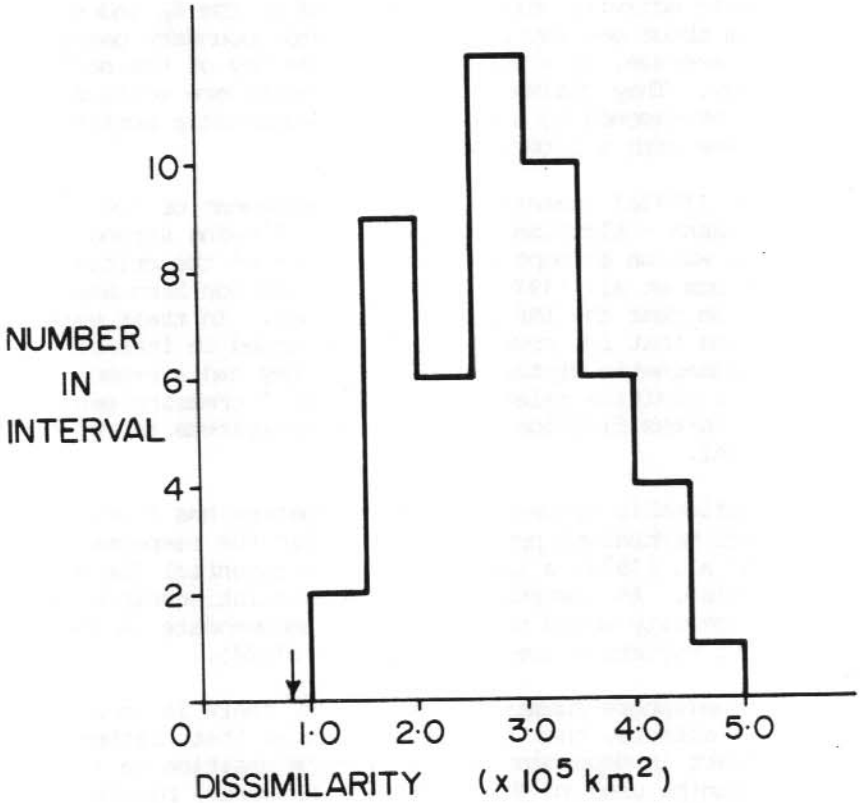

Figure 4. Distribution of 'dissimilarity' values for 50 sets of random curves. The 'dissimilarity' value for the 1.16 x 10^{-4} sec^{-1} threshold curve is arrowed.

7. DISCUSSION OF THE SOUTHERN HEMISPHERE RESULTS

It is not claimed that the above discussion implies that the effect is real. The large number of curves that have been generated may well mean that the claimed correlation of the 1.16×10^{-4} sec^{-1} threshold summer curve with the inverted K_p curve resulted purely by chance. No such tests, as have been described above, would have been necessary if the excursion of the Southern Hemisphere curves were as significant as the Northern Hemisphere result. Evidence against the reality of this effect is that it is not readily apparent in the higher or lower vorticity thresholds analysed (Figure 10).

If the effect is real then the implication is as follows. The fact that the vorticity increases when the geomagnetic activity, as indicated by the K_p index, decreases implies an instantaneous inverse relationship between the two parameters.

Roberts and Olson (1973b) interpreted the relationship between the K_p variation curve and the Northern Hemisphere vorticity response in the following manner. When the sector boundaries pass the earth there is a decrease in the average geomagnetic activity which is reflected by the K_p index. This reaches a minimum about one day before the sector boundary passage. This is followed, on the average, by a sharp rise on the day of the sector passage and the succeeding day. They claimed the dip in hemisphere vorticity and its subsequent rise corresponds to a decrease in geomagnetic activity and its subsequent increase with a 2 to 3 day delay.

Roberts and Olson (1973a) investigated the development of low pressure systems in the Gulf of Alaska - Aleutian Islands area following strong geomagnetic disturbances. It was an attempt to overcome some of the criticisms of this work that led Wilcox et al. (1973) to discover the Northern Hemisphere absolute vorticity variation near the IMF sector crossings. In their work Roberts and Olson (1973a) found that low pressure systems tended to intensify 4 to 5 days after a strong geomagnetic disturbance. Thus they had a reason for suspecting a time delay and a positive relationship between increasing geomagnetic activity and the intensification of low pressure systems as reflected by an increase in the VAI.

The temporal relationship between the two parameters has a bearing on the suitability of the mechanisms proposed to explain the response. From the work of Sommerville et al. (1974) a time delay seems essential for an ozone modulation mechanism. An instantaneous inverse relationship between vorticity and geomagnetic activity would not be hard to accommodate in the global electrical circuit variation theory of Markson (1974).

If the Southern Hemisphere summer effect exists, there is no apparent Southern Hemisphere winter effects, then the implication is that, rather than being seasonal, the effect is dependent on the earth's position in its orbit. The 4 southern summer months used in this analysis (November, December, January and February), are included in the northern winter analysis of Wilcox et al. (1973, 1974, 1975) which also uses data from March. It is interesting that the earth is 3% closer to the sun in January than July due to the slight ellipticity of the earth's orbit. A solar magnetic activity modulation of this 6% increase in incident radiation may be of significance.

8. AN AUSTRALIAN SECTOR ANALYSIS

The Southern Hemisphere meteorological data used in this analysis consists of 500 mb geopotential height values. As the Southern Hemisphere contains large areas of ocean over which few meteorological observations are made, the weather maps, which are digitised to give the grid data, often contain a degree of free-hand interpolation in these regions. The quadrant containing Australia and New Zealand is the region from which the most reliable data are available.

A separate analysis was thus carried out using only data from between 90°E and 180°E longitude and at latitudes greater than 20°S. This area is relatively flat and the vorticity values within this region are less than in the dominating sector east of the Andes. Thus although it is the region of most reliable meteorological data it has only a minor influence on the Southern Hemisphere vorticity area total at high thresholds. The fact that the higher vorticity readings come from regions with less reliable meteorological data may explain the lack of a measureable effect, at high vorticity thresholds, similar to the possible summer low vorticity response previously referred to.

Because of the lower vorticity values occurring in this region, lower thresholds were used to investigate any possible response. The ten thresholds used ranged from 0.30×10^{-4} sec^{-1} to 0.75×10^{-4} sec^{-1} and the associated areas were from 8.0×10^{6} km^2 to 1.0×10^{6} km^2 (from 20% to 2.5% of the quadrant area). Figures 12 to 15 show the superposed epoch analysis results for the Australian sector analysis. This was performed along identical lines to the entire Southern Hemisphere analysis. Tables 6 to 9 compare the ± 6 day excursion values of the IMF data with 50 sets of random key dates in the manner previously described for the Southern Hemisphere analysis.

The smoother variation of the superposed epoch curves is an indication that the data from this region is more reliable. The proposed Southern Hemisphere summer effect is a dip in the VAI with a minimum one day after the boundary crossing. The dominance of this effect in the Australian sector summer curves is evidence for the reality of the effect. Figure 5 shows the best of the Australian sector summer curves, the 0.35×10^{-4} sec^{-1} threshold, averaged VAI curve. It must be remembered that the two data sets are not independent and that the excursion of these curves over the ± 6 day period around the boundary crossing dates is not even greater than the average obtained using random key dates.

A possible winter effect also appears in this analysis. This effect consists of a peak in the VAI at the IMF boundary crossing date. This response is dominant in all the winter Australian sector curves. The most impressive of these curves is the 0.35×10^{-4} sec^{-1} vorticity threshold twelve hourly variation curve (Figure 6). The ± 6 day exursion is only 1.59 σ above the mean of the excursions obtained from 50 sets of random numbers but due to the skew of the distribution of the excursions only 2 of the sets of random numbers result in a greater excursion. Figure 7 shows the distribution of excursion values for this analysis. The reality of the response is in no way conclusive, however, it is worth recording.

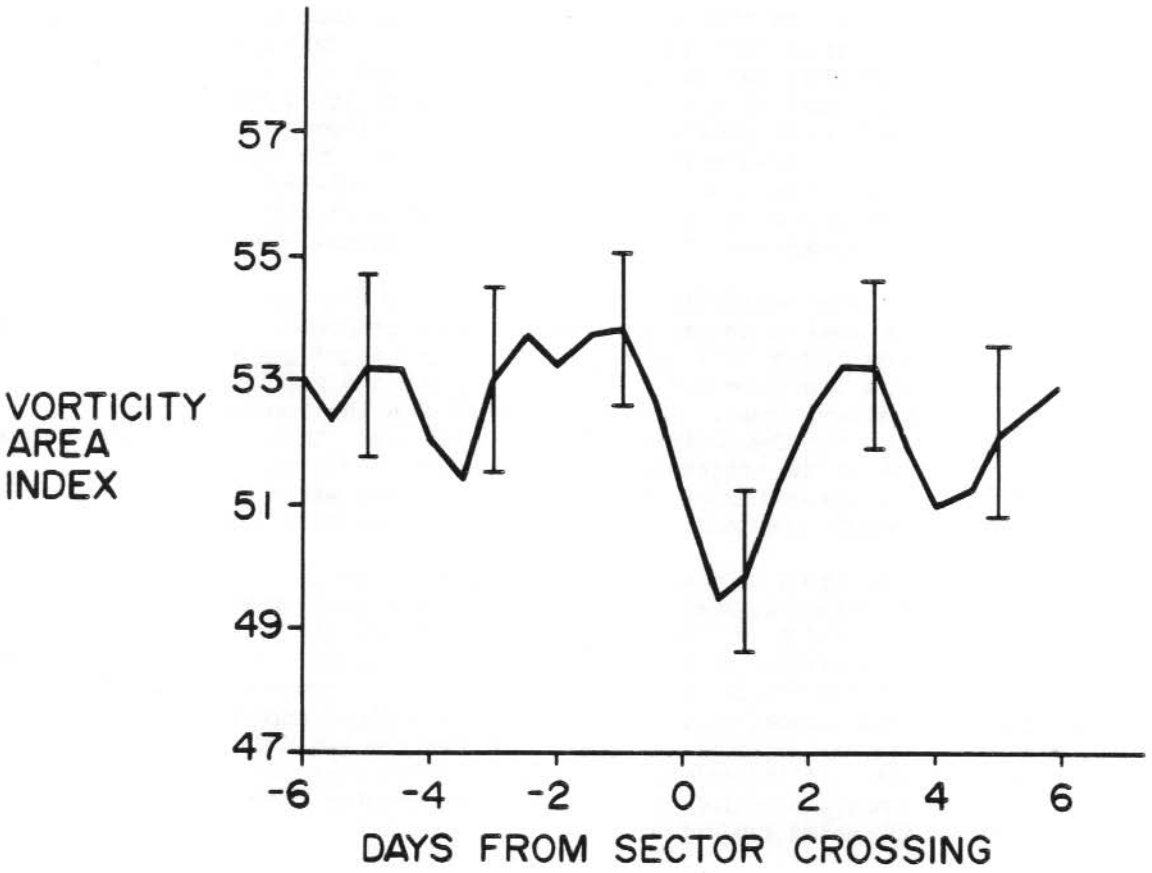

Figure 5. The 0.35 x 10^{-4} sec^{-1} threshold superposed epoch curve for the summer, Australian sector, averaged VAI data.

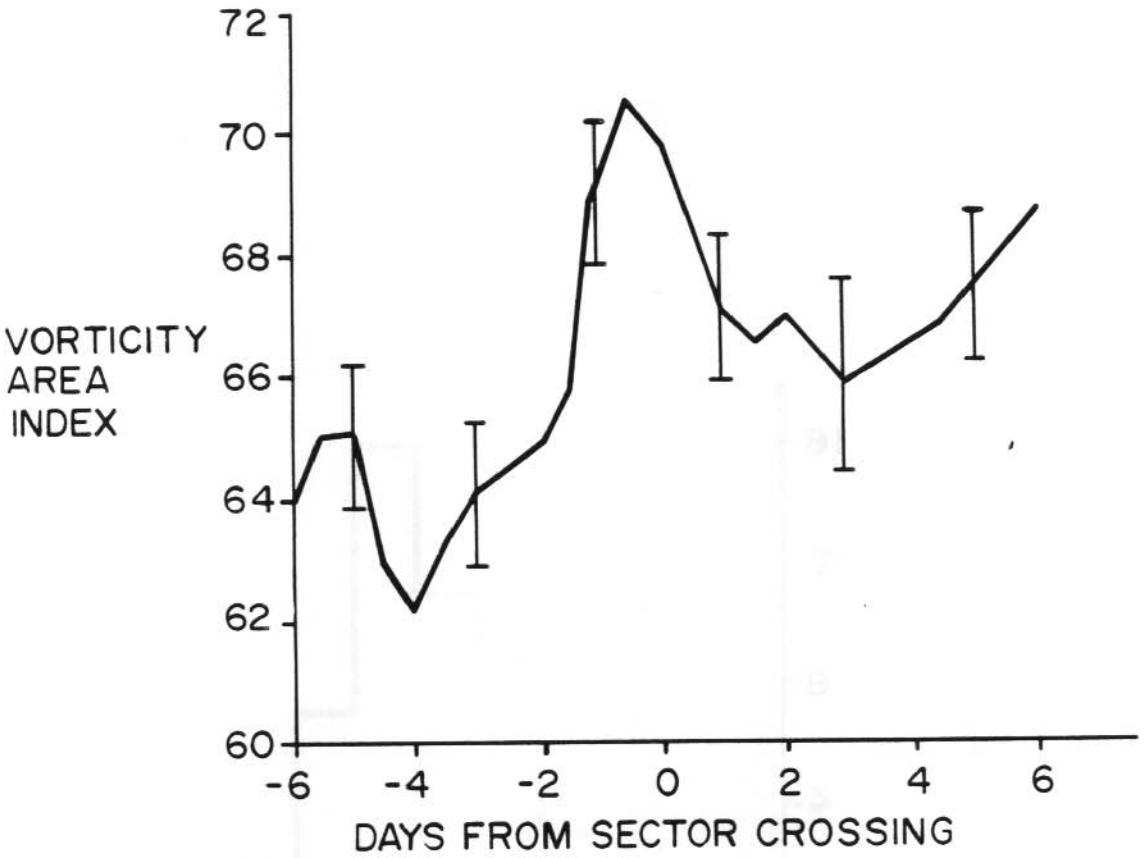

Figure 6. The 0.35 x 10^{-4} sec^{-1} threshold superposed epoch curve for the winter, Australian sector, twelve hourly variation data.

9. SPRING AND AUTUMN DATA

Superposed epoch curves were also calculated for the Southern Hemisphere spring (September, October) and autumn (March, April) two month periods. The limited number of IMF boundary crossings in this period (22 for spring, 21 for which a complete ± 6 days of meteorological data was available and 16 for autumn of which only 13 had complete meteorological data coverage) resulted in widely varying responses. No further analysis of these data was attempted. Figures 16 to 19 show the superposed epoch curves obtained.

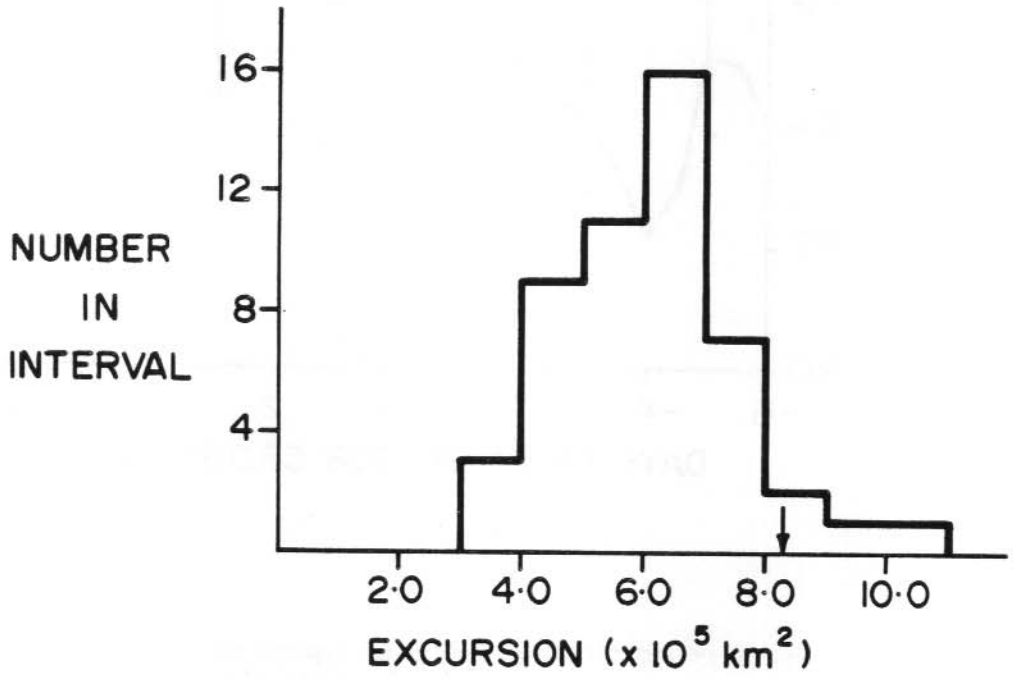

Figure 7. Distribution of the 'excursion' values for 50 random sets of key dates for the winter, Australian sector, twelve-hourly variation data. The excursion of the 0.35 x 10⁻⁴ sec⁻¹ threshold IMF data curve is arrowed.

10. CONCLUSIONS

This investigation has raised the possibility of a Southern Hemisphere vorticity dip near solar sector boundary crossings of the IMF in the summer months. This dip is similar to that obtained by other researchers for the Northern Hemisphere winter. A vorticity peak in the winter months for the Australian quadrant of the Southern Hemisphere is also plausible. The existence of these responses is in no way conclusive.

It was apparent from the beginning of this analysis that the Southern Hemisphere meteorological data is inferior to that available for the Northern Hemisphere. There is reason to hope that, with the present international study of the Southern Ocean, future Southern Hemisphere meteorological data will be more reliable. The use of floating buoys collecting surface pressure and temperature data for transmission to orbiting satellites will improve the meteorological data set.

Hines and Halevy (1977) have pointed out that inaccuracies in determining the boundary crossing dates of the order of 24 hours can completely mask the effect that has been found in the Northern Hemisphere. The boundary crossings inferred by Svalgaard and used in this analysis have an agreement percentage of only 85% (Wilcox, 1972) with satellite determinations of the direction of the IMF. Thus inaccuracies in the determination of the boundary crossing dates may have led to a decrease in the measurable response.

The reality of the proposed responses may be tested when a significantly larger meteorological data bank becomes available.

APPENDIX

This appendix contains all the superposed epoch curves produced by the analysis described in the text and the tables relating to the random key date analysis of the significance of these curves.

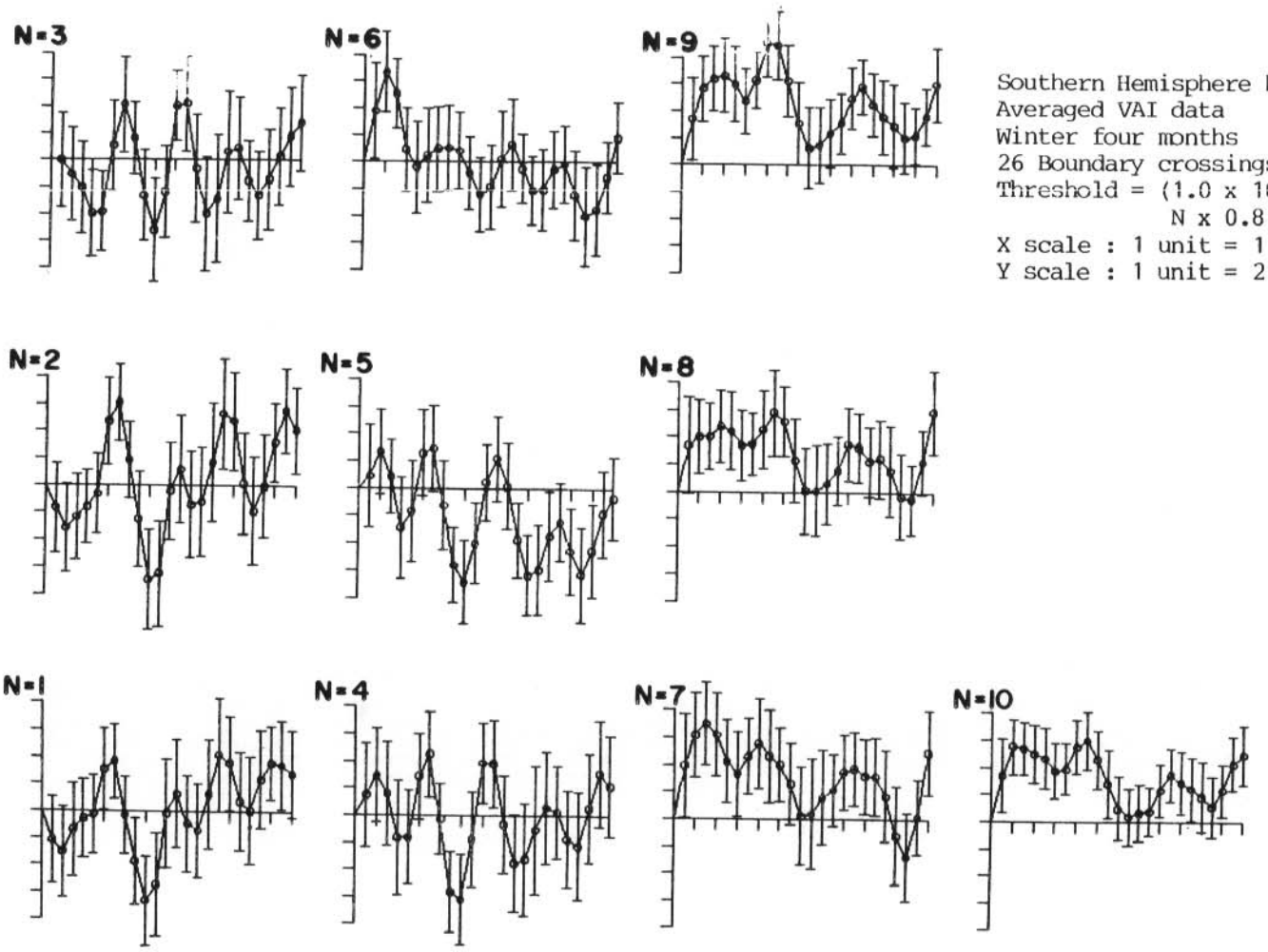

Figure 8. A superposed epoch analysis of the Southern Hemisphere, winter, averaged VAI data for various thresholds, around the solar sector boundary crossings. The date of the boundary crossings is the centre of the x-axis. The data at top right applies to this set of curves.

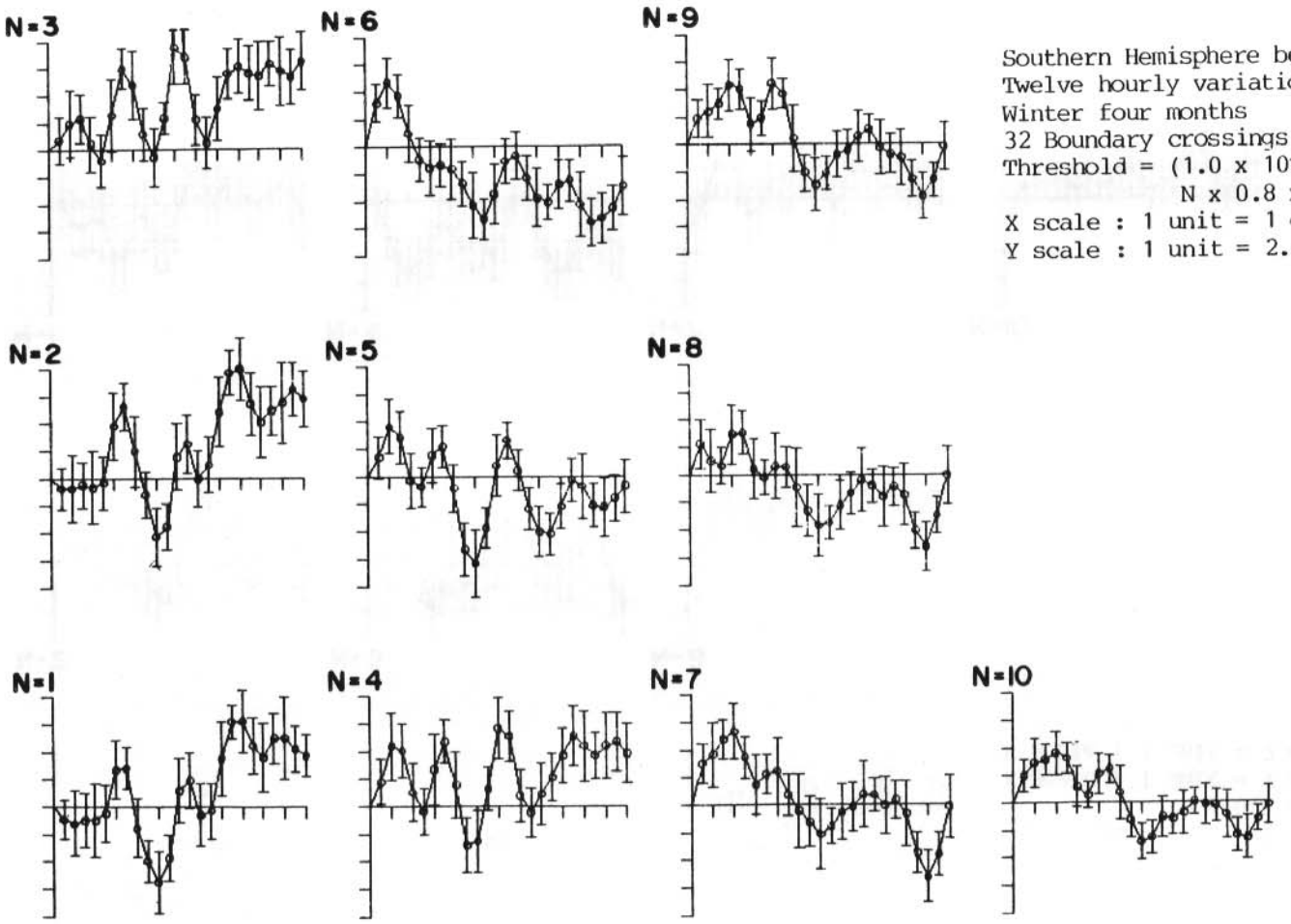

Figure 9. A superposed epoch analysis of the Southern Hemisphere, winter, twelve hourly variation VAI data, for various thresholds, around the solar sector boundary crossings. The date of the boundary crossings is the centre of the x-axis. The data at top right applies to this set of curves.

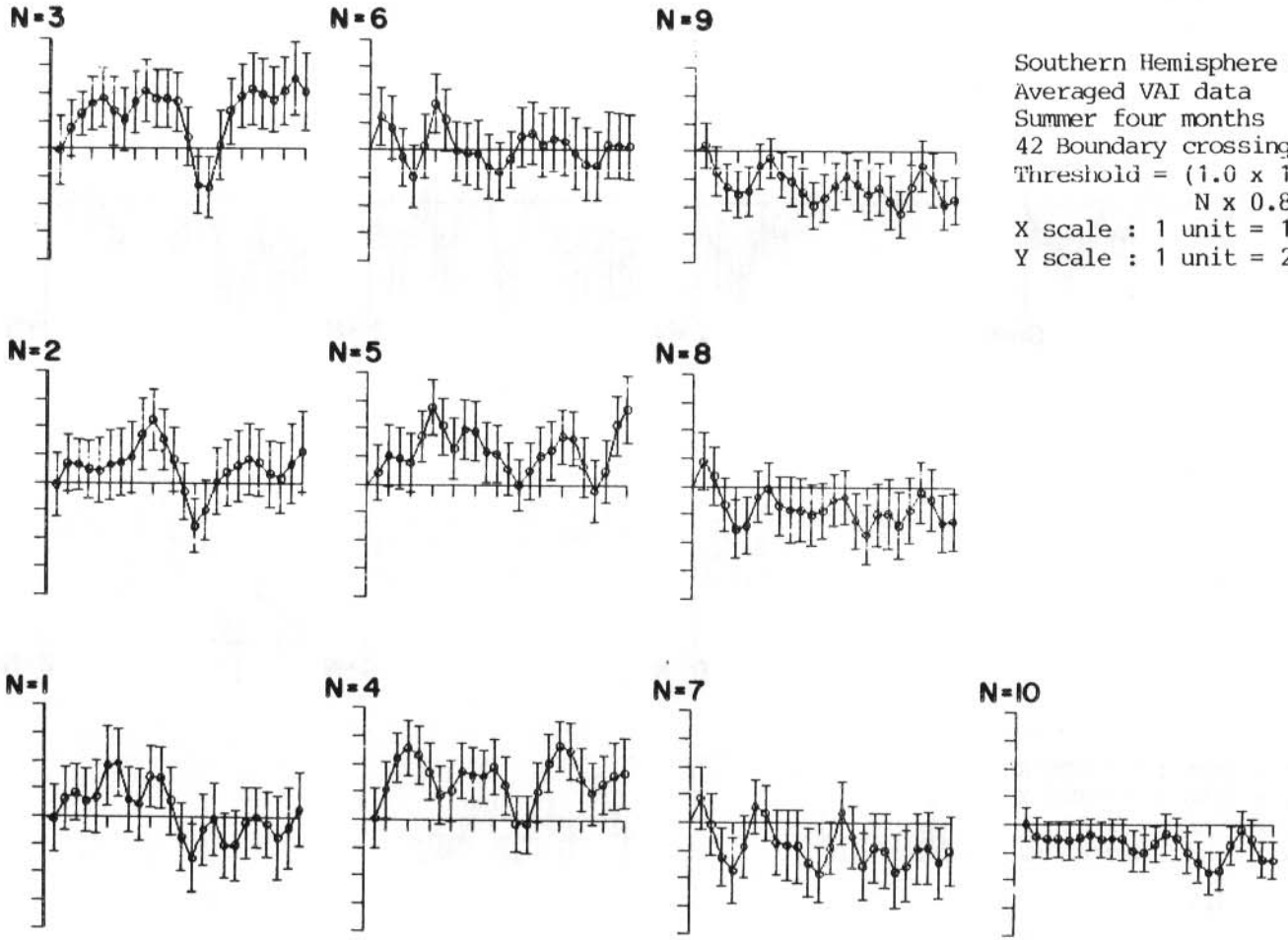

Figure 10. A superposed epoch analysis of the Southern Hemisphere, summer, averaged VAI data for various thresholds, around the solar sector boundary crossings. The date of the boundary crossings is the centre of the x-axis. The data at top right applies to this set of curves.

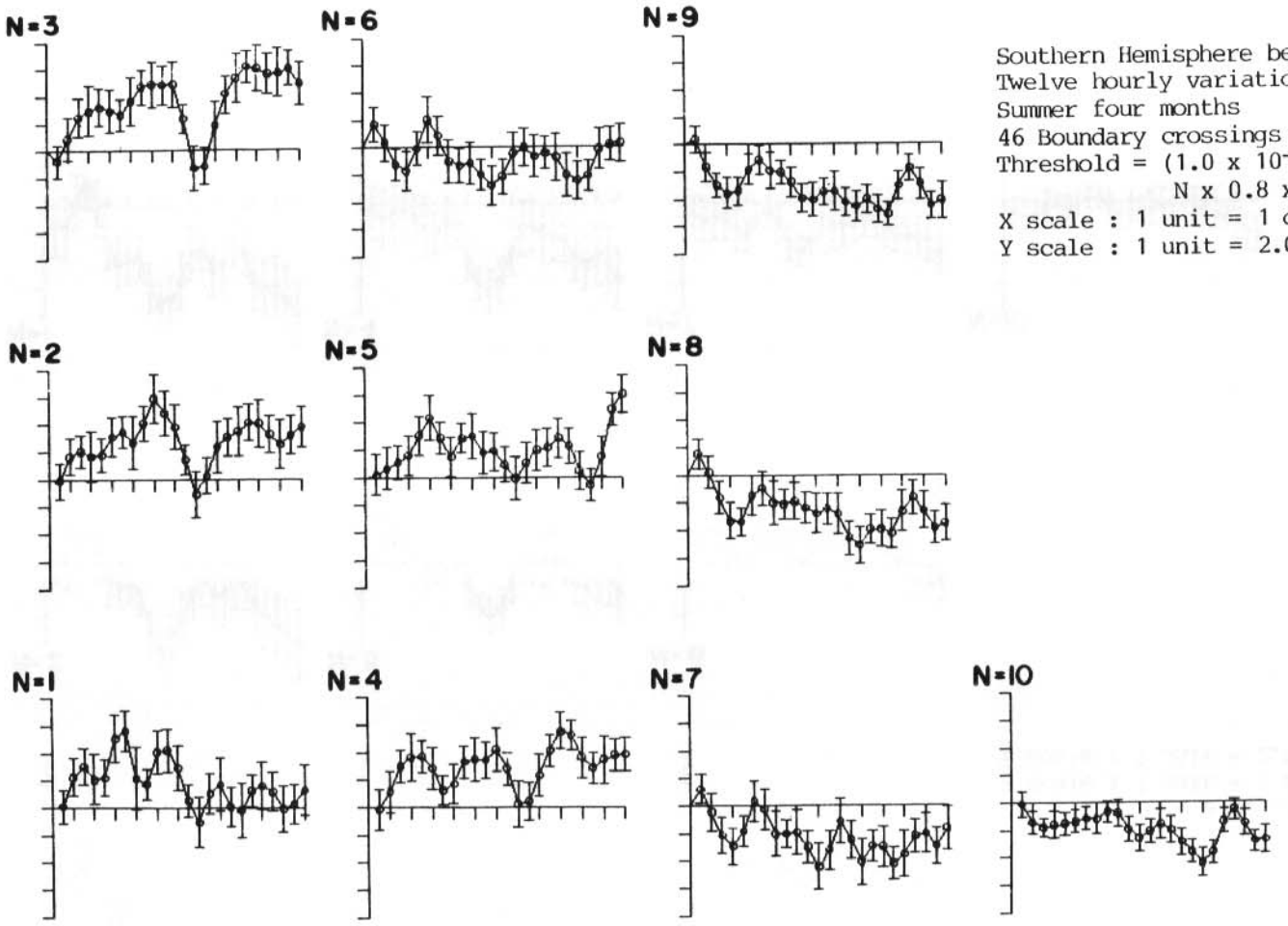

Figure 11. A superposed epoch analysis of the Southern Hemisphere, summer, twelve hourly variation, VAI data for various thresholds, around the solar sector boundary crossings. The date of the boundary crossings is the centre of the x-axis. The data at top right applies to this set of curves.

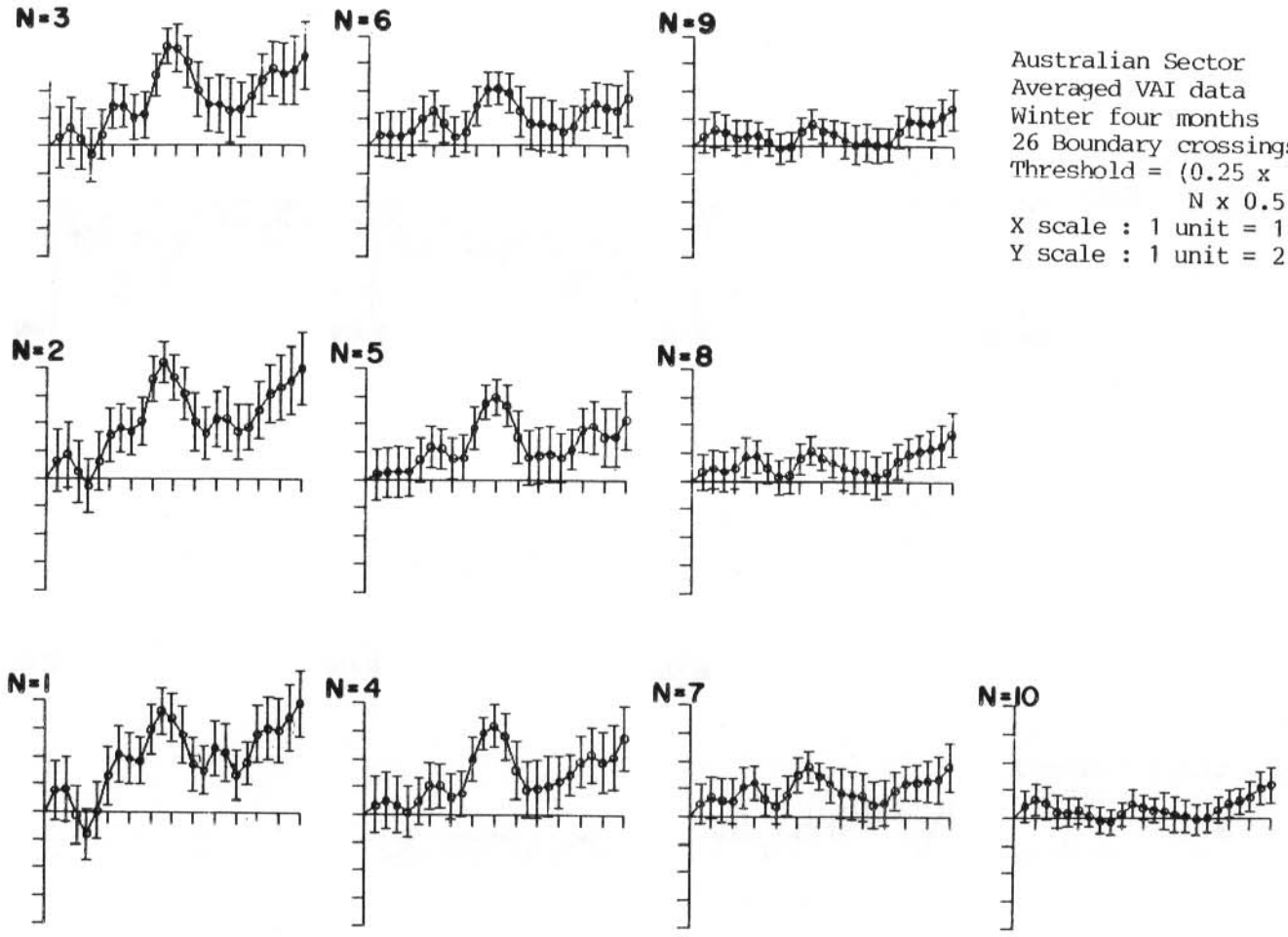

Figure 12. A superposed epoch analysis of the Australian Sector, winter, averaged VAI data for various thresholds, around the solar sector boundary crossings. The date of the boundary crossings is the centre of the x-axis. The data at top right applies to this set of curves.

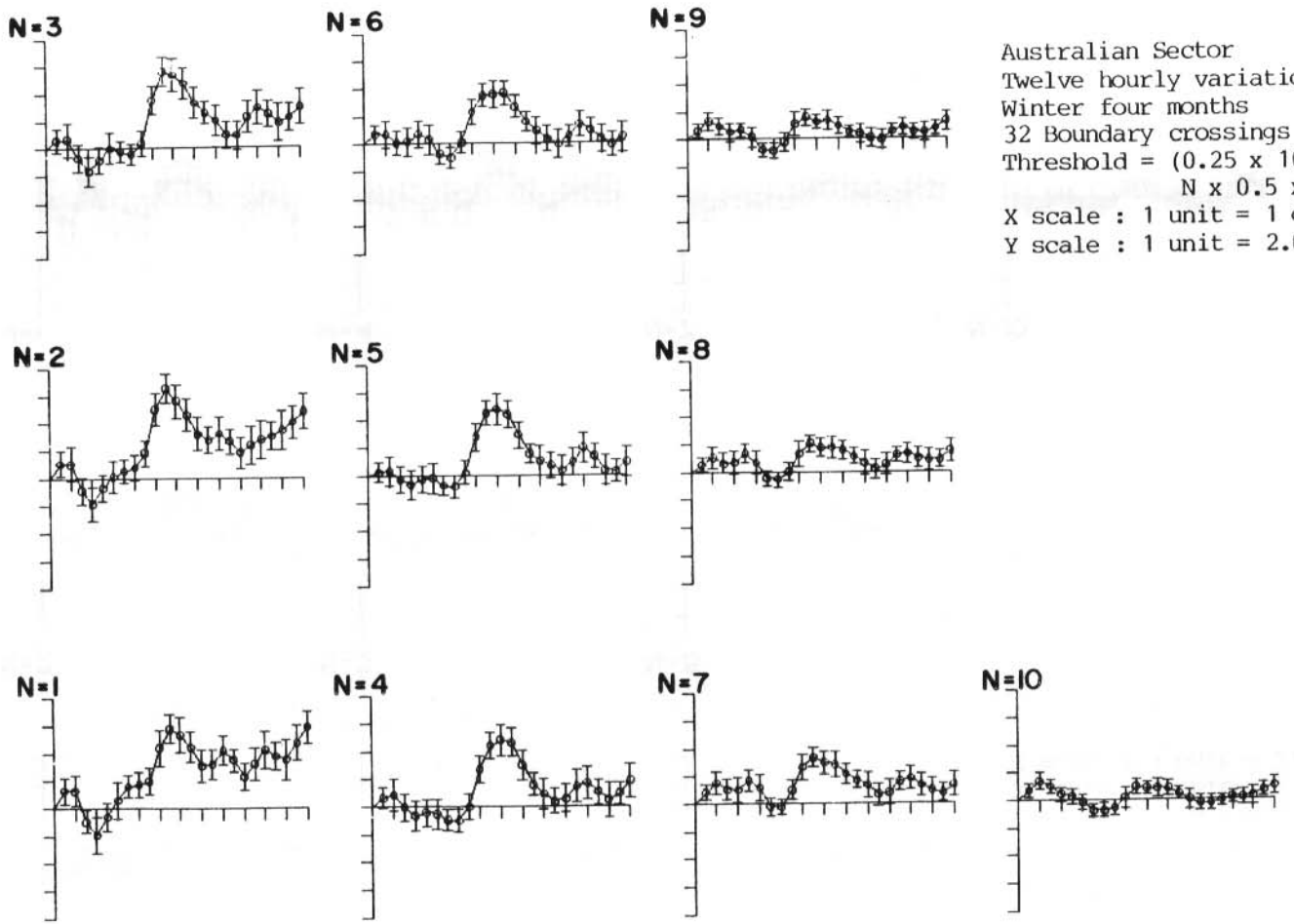

Figure 13. A superposed epoch analysis of the Australian Sector, winter, twelve hourly variation, VAI data for various thresholds, around the solar sector boundary crossings. The date of the boundary crossings is the centre of the x-axis. The data at top right applies to this set of curves.

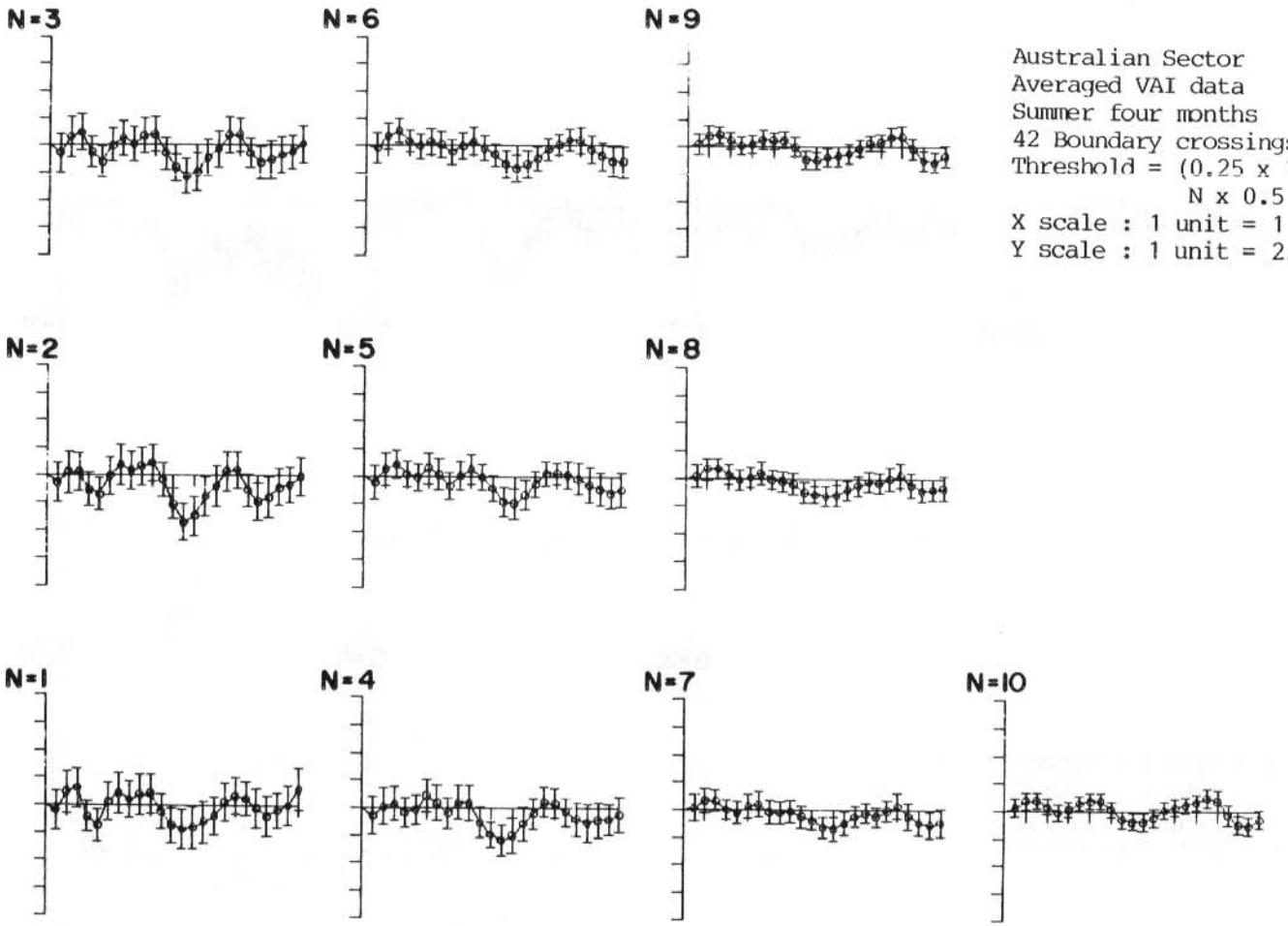

Figure 14. A superposed epoch analysis of the Australian Sector, summer, averaged VAI data for various thresholds, around the solar sector boundary crossings. The date of the boundary crossings is the centre of the x-axis. The data at top right applies to this set of curves.

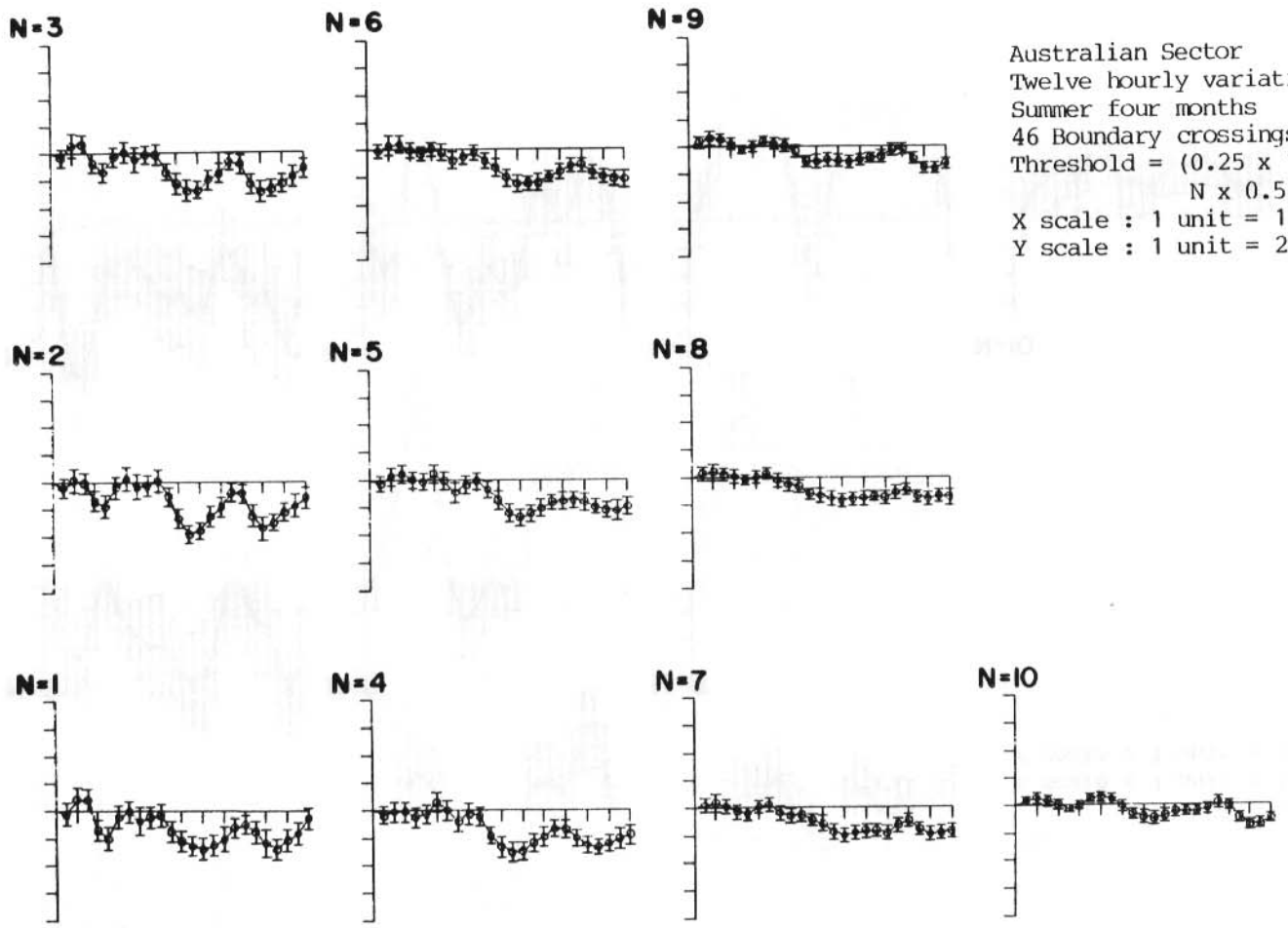

Figure 15. A superposed epoch analysis of the Australian Sector, summer, twelve hourly variation VAI data, for various thresholds, around the solar sector boundary crossings. The date of the boundary crossings is the centre of the x-axis. The data at top right applies to this set of curves.

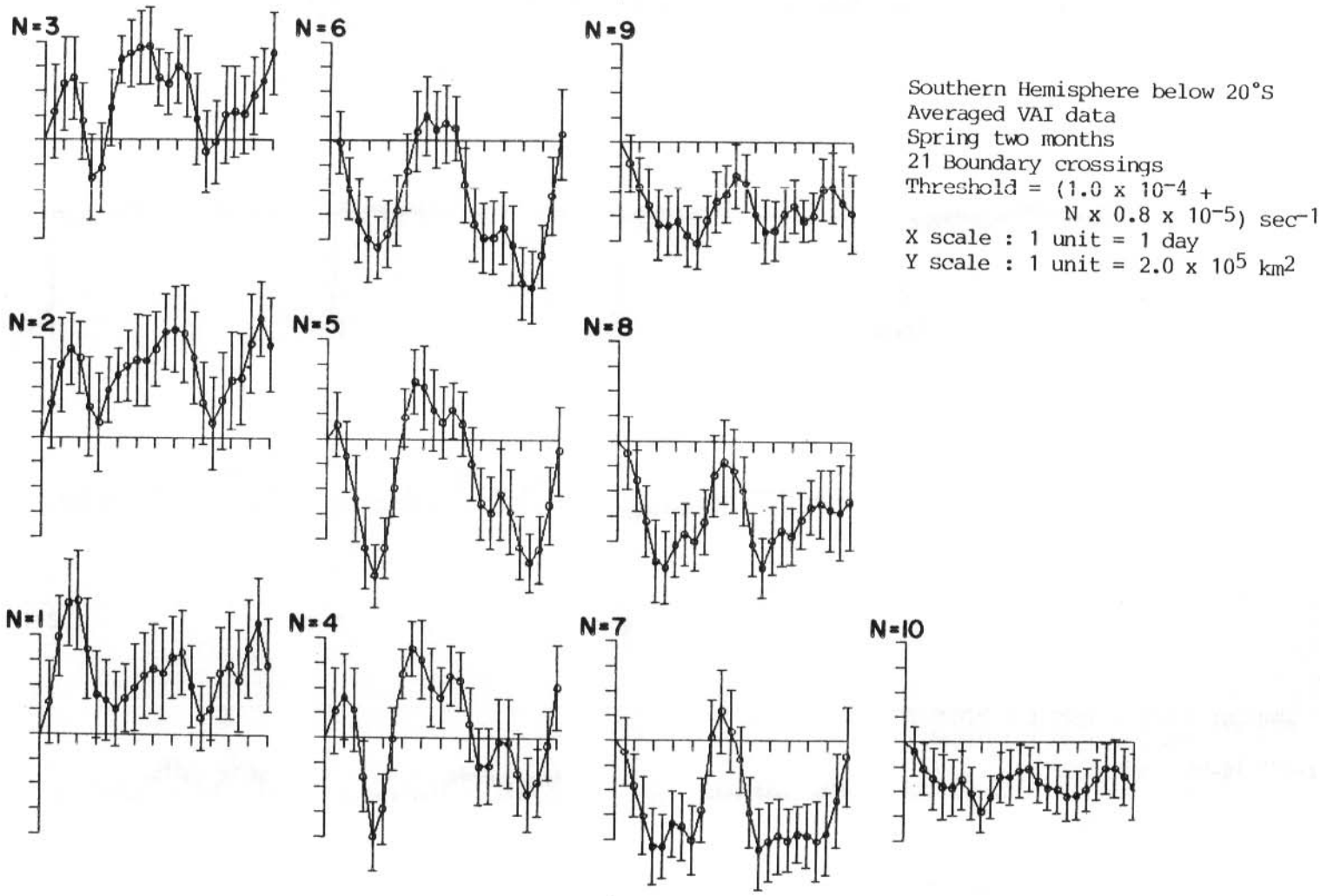

Figure 16. A superposed epoch analysis of the Southern Hemisphere, spring, averaged VAI data for various thresholds, around the solar sector boundary crossings. The date of the boundary crossings is the centre of the x-axis. The data at top right applies to this set of curves.

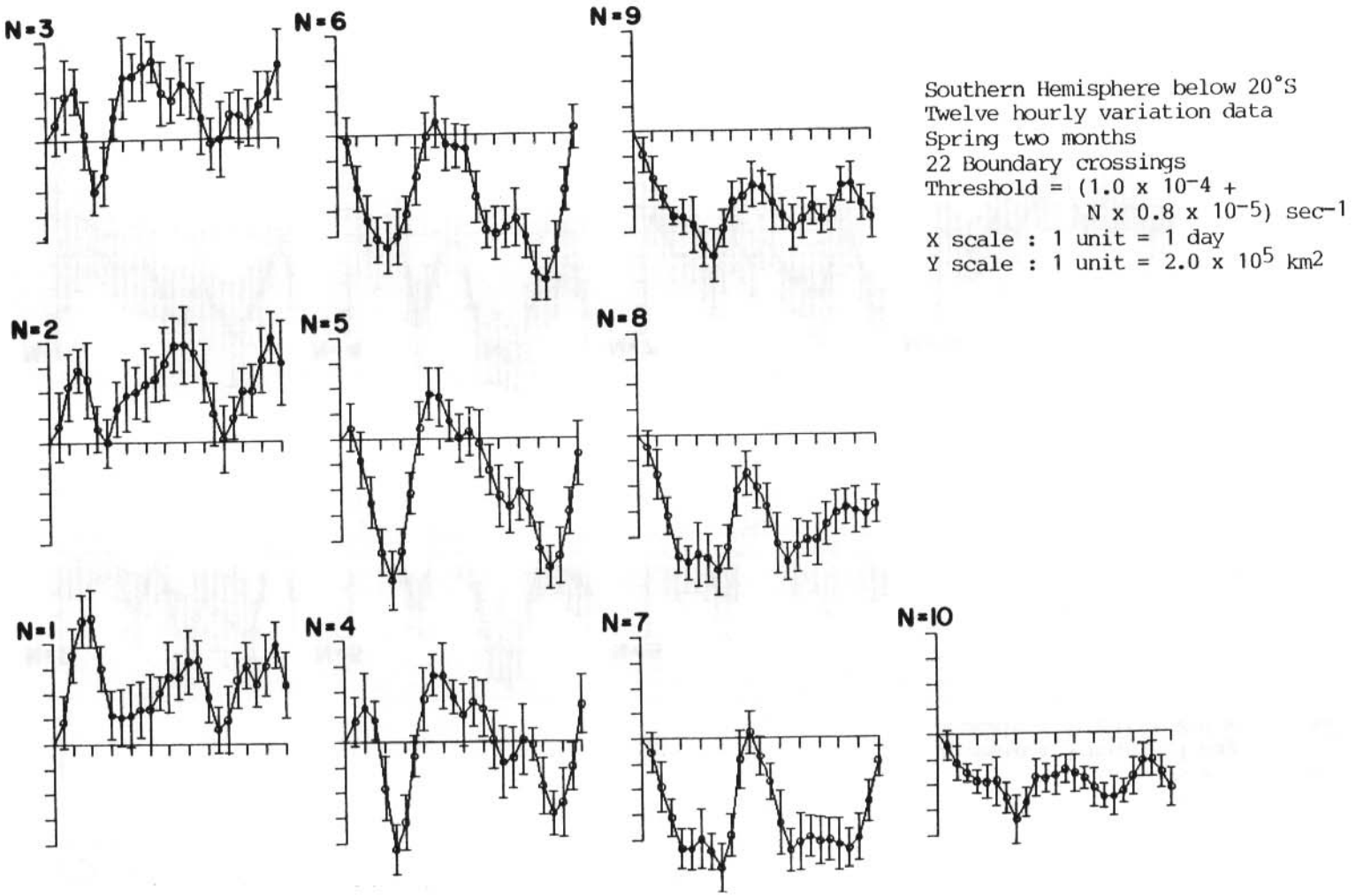

Figure 17. A superposed epoch analysis of the Southern Hemisphere, spring, twelve hourly variation, VAI data for various thresholds, around the solar sector boundary crossings. The date of the boundary crossings is the centre of the x-axis. The data at top right applies to this set of curves.

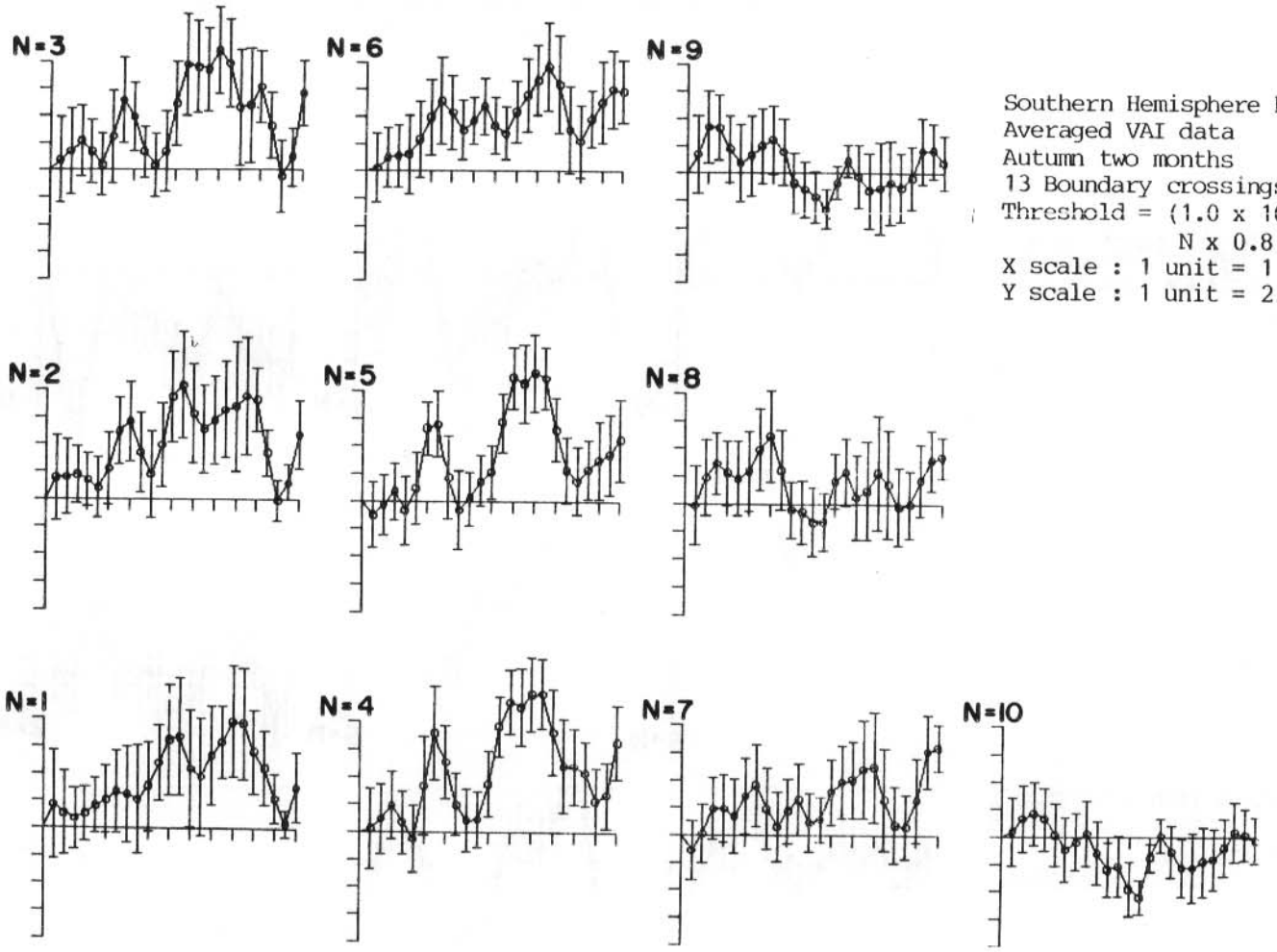

Figure 18. A superposed epoch analysis of the Southern Hemisphere, autumn, averaged VAI data for various thresholds, around the solar sector boundary crossings. The date of the boundary crossings is the centre of the x-axis. The data at top right applies to this set of curves.

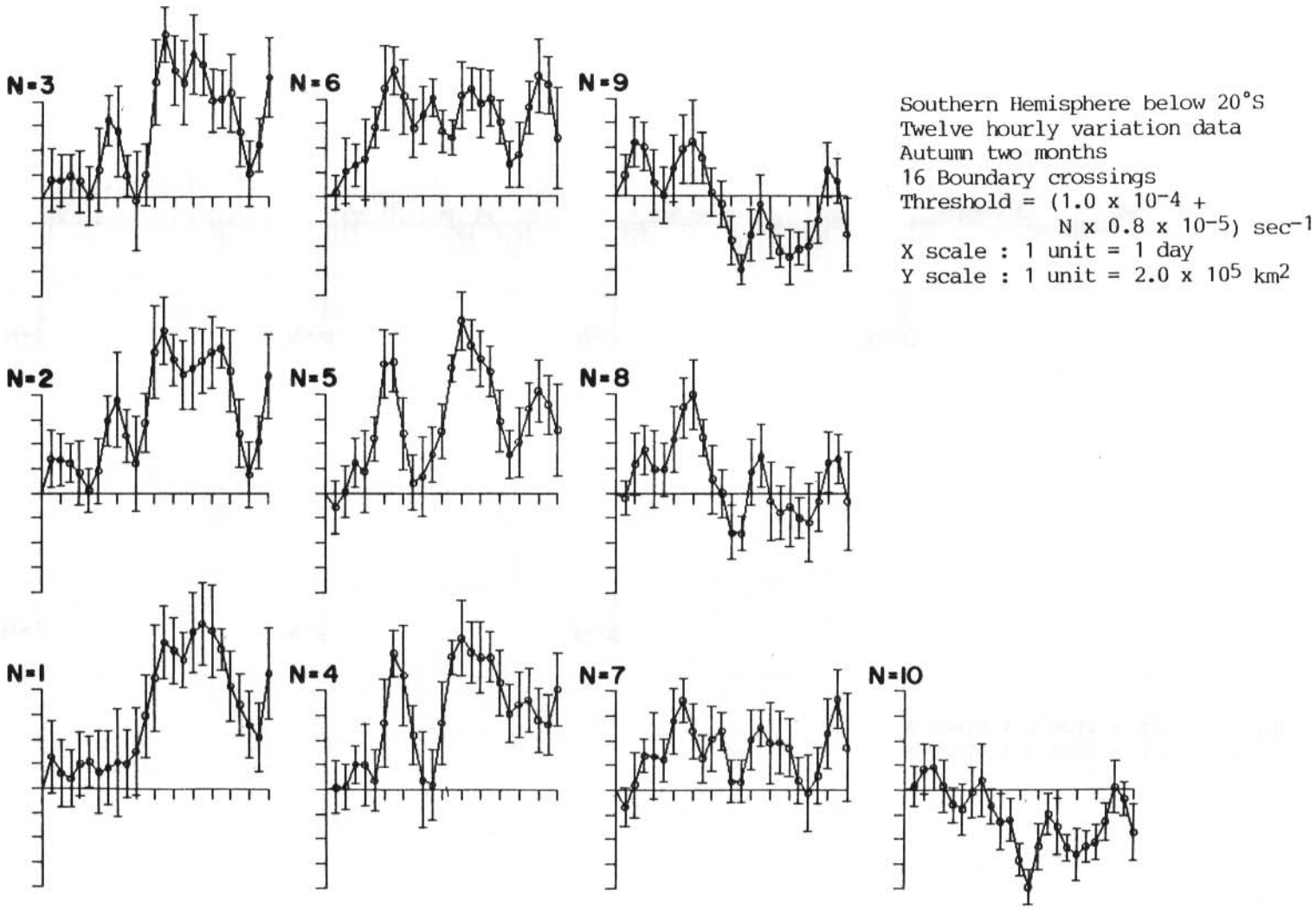

Figure 19. A superposed epoch analysis of the Southern Hemisphere, autumn, twelve hourly variation, VAI data for various thresholds, around the solar sector boundary crossings. The date of the boundary crossings is the centre of the x-axis. The data at top right applies to this set of curves.

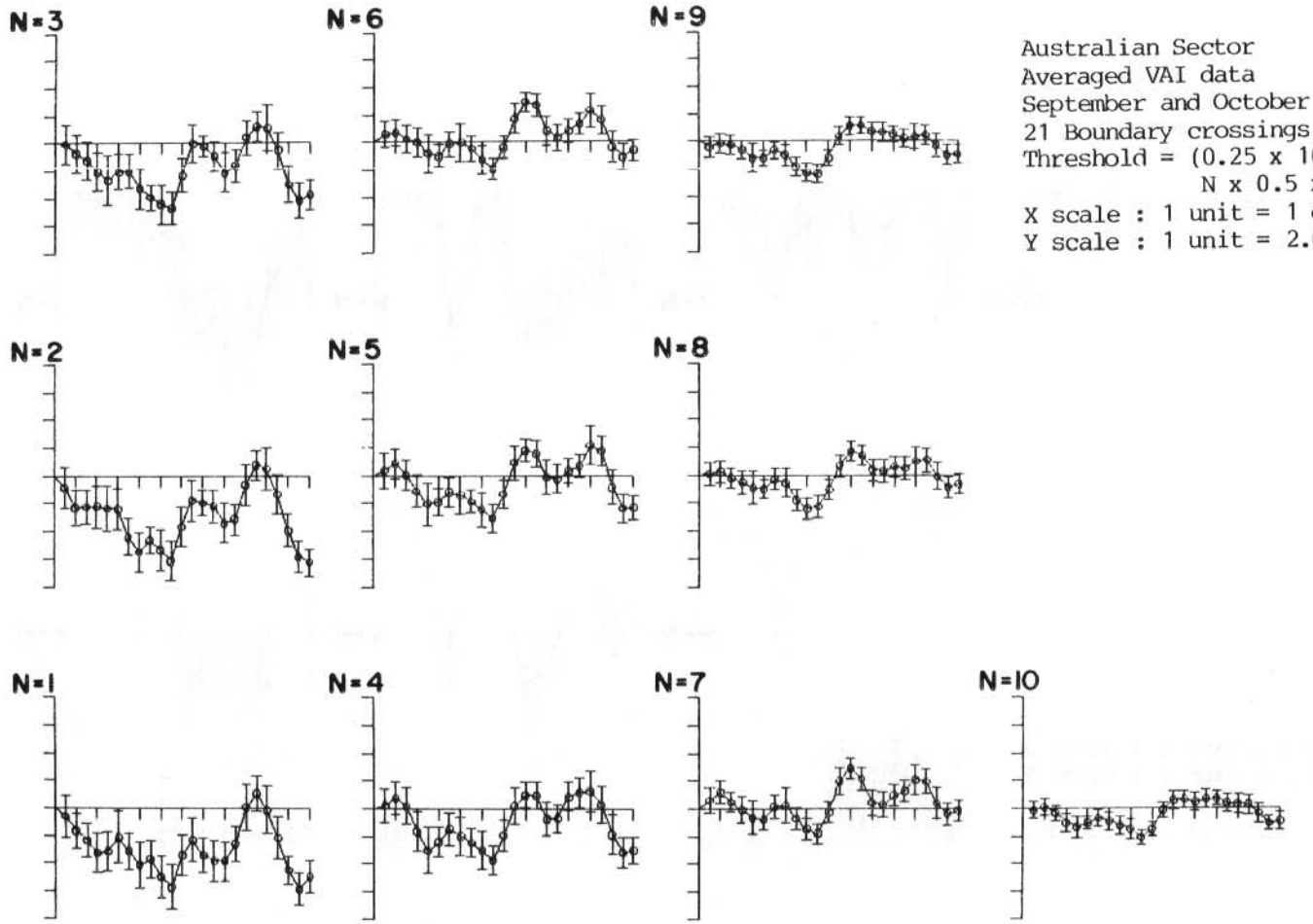

Figure 20. A superposed epoch analysis of the Australian Sector, spring, averaged VAI data for various thresholds, around the solar sector boundary crossings. The date of the boundary crossings is the centre of the x-axis. The data at top right applies to this set of curves.

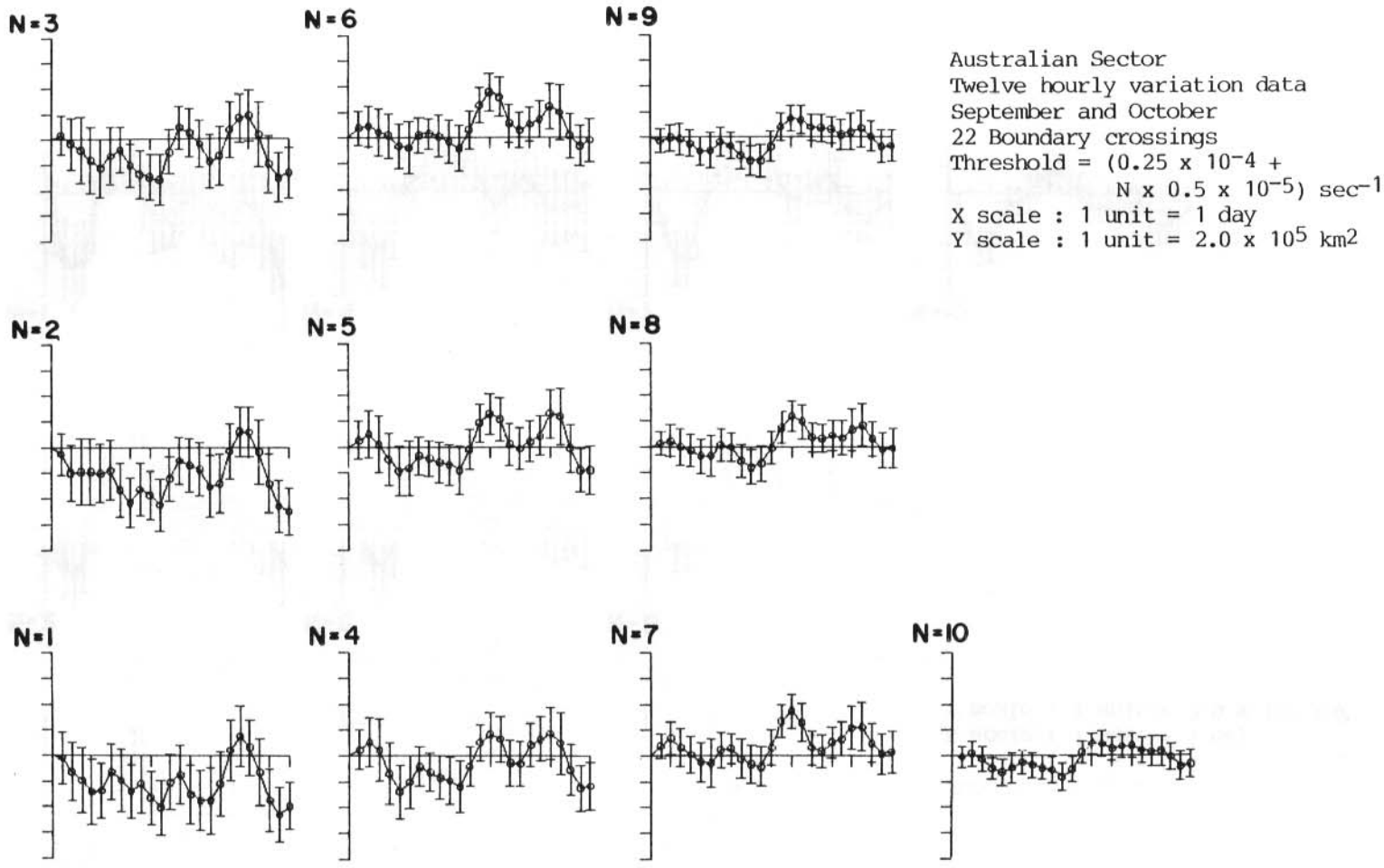

Figure 21. A superposed epoch analysis of the Australian Sector, spring, twelve hourly variation VAI data, for various thresholds, around the solar sector boundary crossings. The date of the boundary crossings is the centre of the x-axis. The data at top right applies to this set of curves.

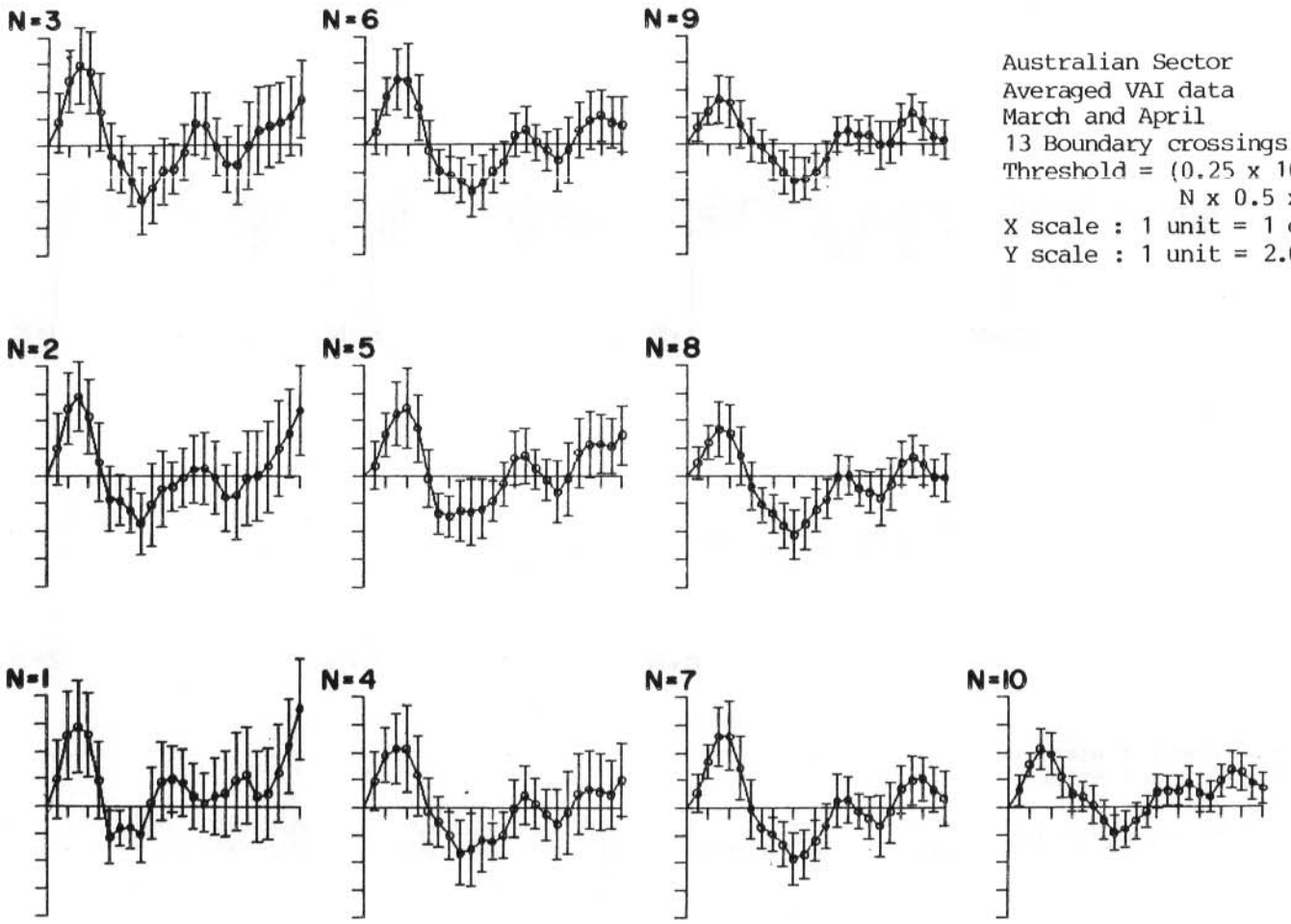

Figure 22. A superposed epoch analysis of the Australian Sector, autumn, averaged VAI data for various thresholds, around the solar sector boundary crossings. The date of the boundary crossings is the centre of the x-axis. The data at top right applies to this set of curves.

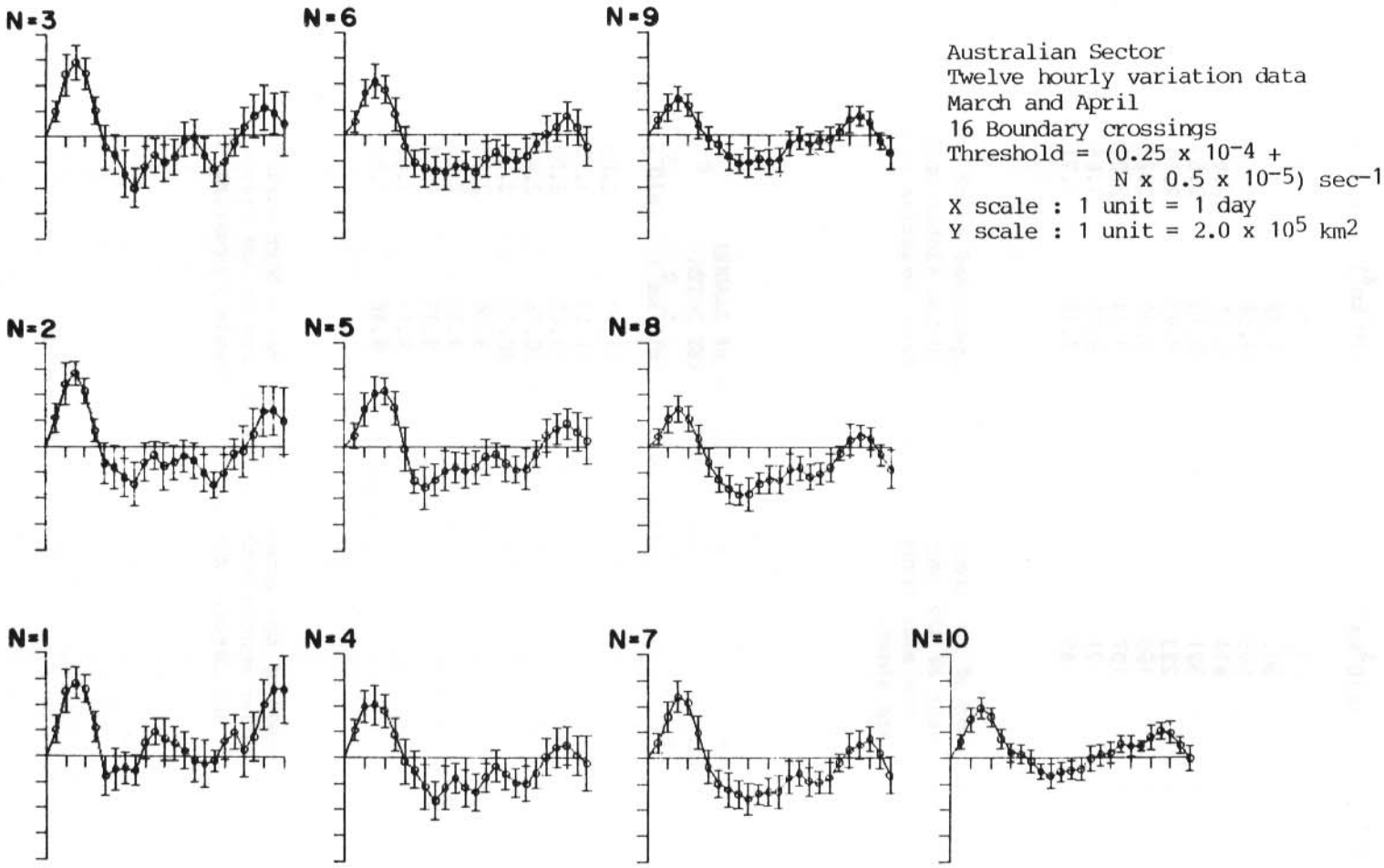

Figure 23. A superposed epoch analysis of the Australian Sector, autumn, twelve hourly variation, VAI data for various thresholds, around the solar sector boundary crossings. The date of the boundary crossings is the centre of the x-axis. The data at top right applies to this set of curves.

N	VORTICITY THRESHOLD ($\times 10^{-4}$ sec^{-1})	Ave VAI ($\times 10^5$ km^2)	x of RANDOM KEY DATES ($\times 10^5$ km^2)	$\bar{x}$ of RANDOM KEY DATES ($\times 10^5$ km^2)	σ ($\times 10^5$ km^2)	$\rho = \frac{x-\bar{x}}{\sigma}$
1	1.08	692	10.77	11.78	2.89	-0.35
2	1.16	603	13.02	11.39	2.22	0.73
3	1.24	508	9.43	11.39	2.68	-0.73
4	1.32	414	10.69	11.31	2.64	-0.23
5	1.40	321	9.78	10.10	2.53	-0.12
6	1.48	233	10.68	9.93	2.16	0.35
7	1.56	160	9.72	9.79	2.22	-0.03
8	1.64	107	6.38	9.38	2.02	-1.49
9	1.72	71	9.01	8.78	1.66	0.65
10	1.80	45	5.99	7.45	1.71	-0.85

Table 1. Comparison of the excursion of the superposed epoch analysis of the 26 complete data sets of IMF sector crossings in the winter months May to August inclusive. The mean excursion and standard deviation of 50 sets of random key dates are shown.

N	VORTICITY THRESHOLD ($\times 10^{-4}$ sec^{-1})	x of RANDOM KEY DATES ($\times 10^5$ km^2)	$\bar{x}$ of RANDOM KEY DATES ($\times 10^5$ km^2)	σ ($\times 10^5$ km^2)	$\rho = \frac{x-\bar{x}}{\sigma}$
1	1.08	11.71	11.27	2.85	0.15
2	1.16	12.23	11.53	3.15	0.22
3	1.24	8.24	11.65	2.59	-1.32
4	1.32	8.46	10.78	2.46	-0.94
5	1.40	9.97	10.15	2.36	-0.08
6	1.48	10.27	9.86	2.53	0.16
7	1.56	10.65	9.57	2.22	0.49
8	1.64	8.32	9.17	1.94	-0.44
9	1.72	8.22	8.11	1.82	0.06
10	1.80	6.46	6.66	1.55	-0.13

Table 2. Comparison of the excursion of the twelve hour variation in VAI curves for the winter months with the mean excursion and standard deviation of 50 sets of random key dates. A total of 32 boundary crossing dates were used in this analysis.

N	VORTICITY THRESHOLD ($\times 10^{-4}$ sec^{-1})	Ave VAI ($\times 10^{5}$ km^{2})	x of RANDOM KEY DATES ($\times 10^{5}$ km^{2})	$\bar{x}$ of RANDOM KEY DATES ($\times 10^{5}$ km^{2})	σ ($\times 10^{5}$ km^{2})	$\rho = \frac{x-\bar{x}}{\sigma}$
1	1.08	671	6.80	9.24	1.93	-1.26
2	1.16	591	7.56	8.32	1.72	-0.44
3	1.24	505	7.90	7.58	1.75	0.18
4	1.32	411	5.62	7.00	1.60	-0.86
5	1.40	313	5.97	7.01	1.37	-0.76
6	1.48	218	5.27	7.52	1.59	-1.42
7	1.56	143	5.38	7.60	1.65	-1.35
8	1.64	91	5.15	7.09	1.61	-1.20
9	1.72	57	4.88	6.12	1.44	-0.86
10	1.80	36	3.46	5.00	1.07	-1.44

Table 3. Comparison of the excursion of the superposed epoch analysis of the 42 complete data sets of IMF sector crossings in the summer months November to February inclusive. The mean excursion and standard deviation of 100 sets of random key dates are included.

N	VORTICITY THRESHOLD ($\times 10^{-4}$ sec^{-1})	x of RANDOM KEY DATES ($\times 10^{5}$ km^{2})	$\bar{x}$ of RANDOM KEY DATES ($\times 10^{5}$ km^{2})	σ ($\times 10^{5}$ km^{2})	$\rho = \frac{x-\bar{x}}{\sigma}$
1	1.08	6.66	8.16	1.81	-0.83
2	1.16	6.96	7.76	1.71	-0.45
3	1.24	7.40	7.28	1.83	0.07
4	1.32	5.67	6.55	1.65	-0.53
5	1.40	6.60	6.70	1.48	-0.07
6	1.48	4.85	7.21	1.60	-1.48
7	1.56	5.65	7.54	1.73	-1.09
8	1.64	6.65	6.88	1.52	-0.15
9	1.72	5.45	5.94	1.22	-0.40
10	1.80	4.28	4.96	1.20	-0.57

Table 4. Comparison of the excursion of the twelve hour variation in VAI curves for the summer months with the mean excursion and standard deviation of 50 sets of random key dates. A total of 46 boundary crossing dates were used in this analysis.

N	VORTICITY THRESHOLD ($\times 10^{-4}$ sec^{-1})	Ave VAI ($\times 10^5$ km^2)	x of RANDOM KEY DATES ($\times 10^5$ km^2)	$\bar{x}$ of RANDOM KEY DATES ($\times 10^5$ km^2)	σ ($\times 10^5$ km^2)	$\rho = \frac{x-\bar{x}}{\sigma}$
1	1.08	671	5.82	4.06	2.16	0.81
2	1.16	591	7.56	3.90	2.09	1.75
3	1.24	505	6.26	3.80	2.13	1.15
4	1.32	411	4.04	3.02	1.38	0.74
5	1.40	313	3.79	2.92	1.34	0.78
6	1.48	218	2.53	3.51	1.54	-0.64
7	1.56	143	4.39	3.63	1.68	0.45
8	1.64	91	1.25	3.35	1.67	-1.26
9	1.72	57	2.09	2.96	1.33	-0.65
10	1.80	36	1.32	2.37	1.01	-1.04

Table 5. As for Table 3 but the excursion was calculated for the interval ±1 day from the IMF crossing date as compared with ±6 days in the previous analysis.

N	VORTICITY THRESHOLD ($\times 10^{-4}$ sec^{-1})	Ave VAI ($\times 10^5$ km^2)	x of RANDOM KEY DATES ($\times 10^5$ km^2)	$\bar{x}$ of RANDOM KEY DATES ($\times 10^5$ km^2)	σ ($\times 10^5$ km^2)	$\rho = \frac{x-\bar{x}}{\sigma}$
1	0.30	81.0	9.48	6.89	1.65	1.57
2	0.35	66.9	8.87	6.69	1.47	1.48
3	0.40	55.2	7.86	6.14	1.53	1.12
4	0.45	45.1	6.38	6.01	1.42	0.26
5	0.50	36.5	5.93	5.63	1.34	0.22
6	0.55	29.2	4.14	5.33	1.25	-0.94
7	0.60	23.8	3.60	4.82	1.17	-1.04
8	0.65	19.3	3.39	4.41	0.99	-1.03
9	0.70	15.6	2.92	3.86	0.80	-1.18
10	0.75	12.5	2.72	3.55	0.68	-1.22

Table 6. Comparison of the excursion of the superposed epoch analysis of the 26 complete data sets of IMF sector crossings in the winter months with the mean excursion and standard deviation of 50 sets of random key dates. This analysis refers to the Australian sector data.

N	VORTICITY THRESHOLD ($x10^{-4}sec^{-1}$)	x of RANDOM KEY DATES ($x10^5km^2$)	$\bar{x}$ of RANDOM KEY DATES ($x10^5km^2$)	σ ($x10^5km^2$)	$\rho = \frac{x-\bar{x}}{\sigma}$
1	0.30	7.81	6.37	1.51	0.95
2	0.35	8.34	6.20	1.35	1.59
3	0.40	7.18	5.65	1.32	1.16
4	0.45	5.82	5.43	1.34	0.29
5	0.50	5.56	5.01	1.21	0.45
6	0.55	4.65	4.67	1.18	-0.02
7	0.60	3.57	4.30	1.10	-0.66
8	0.65	2.57	3.99	1.03	-1.38
9	0.70	2.40	3.43	1.01	-1.02
10	0.75	2.13	3.21	0.91	-1.13

Table 7. Comparison of the excursion of the twelve hour variation in VAI curves for the winter months with the mean excursion and standard deviation of 50 sets of random key dates. A total of 32 boundary crossings were used in this analysis which refers to the Australian quadrant below 20°S.

N	VORTICITY THRESHOLD ($x10^{-4}sec^{-1}$)	Ave VAI ($x10^5km^2$)	x of RANDOM KEY DATES ($x10^5km^2$)	$\bar{x}$ of RANDOM KEY DATES ($x10^5km^2$)	σ ($x10^5km^2$)	$\rho = \frac{x-\bar{x}}{\sigma}$
1	0.30	63.9	2.96	4.55	1.07	-1.49
2	0.35	51.8	4.29	4.32	1.07	-0.03
3	0.40	42.2	3.16	4.18	1.01	-1.01
4	0.45	34.1	3.20	3.93	0.92	-0.79
5	0.50	27.4	2.78	3.46	0.83	-0.82
6	0.55	22.1	2.72	3.18	0.76	-0.61
7	0.60	17.8	2.07	2.87	0.67	-1.19
8	0.65	14.4	1.93	2.63	0.45	-1.56
9	0.70	11.3	1.99	2.29	0.40	-0.75
10	0.75	9.1	2.02	2.08	0.37	-0.16

Table 8. Comparison of the excursion of the superposed epoch analysis of the 42 complete data sets of IMF sector crossings in the summer months with the mean excursion and standard deviation of 50 sets of random key dates. This analysis refers to the Australian sector data.

N	VORTICITY THRESHOLD ($\times 10^{-4}$ sec^{-1})	x of RANDOM KEY DATES ($\times 10^5$ km^2)	$\bar{x}$ of RANDOM KEY DATES ($\times 10^5$ km^2)	σ ($\times 10^5$ km^2)	$\rho = \frac{x-\bar{x}}{\sigma}$
1	0.30	3.63	5.06	1.04	-1.38
2	0.35	4.02	4.89	1.01	-0.86
3	0.40	3.55	4.68	0.98	-1.15
4	0.45	3.66	4.47	0.96	-0.84
5	0.50	3.20	4.11	1.04	-0.88
6	0.55	2.94	3.82	1.01	-0.87
7	0.60	2.37	3.36	0.86	-1.15
8	0.65	2.07	2.90	0.78	-1.06
9	0.70	2.25	2.52	0.69	-0.39
10	0.75	2.05	2.32	0.71	-0.38

Table 9. Comparison of the excursion of the twelve hour variation in VAI curves for the summer months with the mean excursion and standard deviation of 50 sets of random key dates. 46 boundary crossing dates were used in this analysis which refers to the Australian sector data.

REFERENCES

Hines, C.O. (1973). Comments on "A test of an apparent response of the lower atmosphere to solar corpuscular radiation". Journal of the Atmospheric Sciences 30:739-740.

Hines, C.O. and Halevy, I. (1977). On the reality and nature of a certain sun-weather correlation. Journal of the Atmospheric Sciences 34:382-404.

Mansurov, S.M. (1969). New evidence of a relationship between magnetic fields in space and on earth. Geomagnetism and Aeronomy (English Translation) 9:622-623.

Markson, R. (1974). Solar modulation of atmospheric electrification through variation of the conductivity over thunder storms. In: Bandeen, W R and Maran, S P (eds.) Proceedings of the Symposium on Possible Relationships Between Solar Activity and Meteorological Phenomena. Greenbelt, Maryland, NASA-Goddard Space Flight Center: 272.

Roberts, W.O. and Olson, R.H. (1973a). Geomagnetic storms and wintertime 300 mb trough development in the North Pacific-North America area. Journal of the Atmospheric Sciences 30:135-140.

Roberts, W.O. and Olson, R.H. (1973b). New evidence for effects of variable solar corpuscular emission on the weather. Reviews of Geophysics and Space Physics 11:731-740.

Shapiro, R. (1976). Solar magnetic sector structure and terrestrial atmospheric vorticity. Journal of the Atmospheric Sciences 33:865-870.

Somerville, R.C.J.; Hanson, J.E.; Stone, P.H.; Quirk, W.J. and Lacis, A.A. (1974). In: Bandeen, W.R. and Maran, S.P. (eds.) Proceedings on the Symposium on Possible Relationships Between Solar Activity and Meteorological Phenomena. Greenbelt, Maryland, NASA-Goddard Space Flight Center: 319.

Svalgaard, L. (1968). Sector structure of the interplanetary magnetic field and daily variation of the geomagnetic field at high latitudes. Geophysical Research Paper R-6. Danish Meteorological Institute, Copenhagen. 11 pp.

Svalgaard, L. (1972). Interplanetary magnetic sector structure, 1926-1971. Journal of Geophysical Reseach 77:4027-4034.

Wilcox, J.M. (1972). Inferring the interplanetary magnetic field by observing the polar geomagnetic field. Reviews of Geophysics and Space Physics 10:1003-1014.

Wilcox, J.M. and Colburn, D.S. (1972). Interplanetary sector structure at solar maximum. Journal of Geophysical Research 77:751-756.

Wilcox, J.M.; Scherrer, P.H.; Svalgaard, L.; Roberts, W.O. and Olson, R.H. (1973). Solar magnetic sector structure: relation to the earth's atmosphere. Science 180:185-186.

Wilcox, J.M.; Scherrer, P.H.; Svalgaard, L.; Roberts, W.O.; Olson, R.H. and Jenne, R.L. (1974). Influence on solar magentic sector structure on terrestrial atmospheric vorticity. Journal of the Atmospheric Sciences 31:581-588.

Wilcox, J.M.; Svalgaard, L. and Scherrer, P.H. (1975). Seasonal variation and magnitude of the solar sector structure - atmospheric vorticity effect. Nature 255:539-540.

Wilcox, J.M.; Svalgaard, L. and Scherrer, P.H. (1976). On the reality of a sun-weather effect. Journal of the Atmospheric Sciences 33:1113-1116.

ACKNOWLEDGMENTS

Major F.R. Bond, who suggested this project, and Dr J.S. Reid, both formerly of the Antarctic Division, Department of Science and Technology, provided helpful discussions and advice throughout this study.

Thanks are due to the Bureau of Meteorology, Department of Science and Technology, which provided the geopotential height grid data used in this analysis and to Mr R. Falconer who advised on the availability and accuracy of the data. Professor L. Svalgaard of Stanford University provided the inferred solar sector crossing data.

This project was carried out on the LaTrobe University DEC 10 computer system, access to which assisted in the rapid analysis of data. The suggestions of, and discussions with, Professor K.D. Cole throughout this project have proved invaluable.

Mr H. Burton has assisted with advice on the foibles of the DEC 10 computer system and wrote the random key date generation program used in this analysis.

ANARE RESEARCH NOTES (ISSN 0729-6533)

1. John M. Kirkwood (1982). A guide to the Euphausiacea of the Southern Ocean.

2. David O'Sullivan (1982). A guide to the Chaetognaths of the Southern Ocean and adjacent waters.

3. David O'Sullivan (1982). A guide to the Pelagic Polychaetes of the Southern Ocean and adjacent waters.

4. David O'Sullivan (1982). A guide to the Scyphomedusae of the Southern Ocean and adjacent waters.

5. David O'Sullivan (1982). A guide to the Hydromedusae of the Southern Ocean and adjacent waters.

6. Paul J. McDonald (1983). Steam aided curing of concrete in Antarctica.

7. Richard Williams, John M. Kirkwood, David O'Sullivan (1983). FIBEX cruise zooplankton data.

8. David O'Sullivan (1983). A guide to the Pelagic Tunicates of the Southern Ocean and adjacent waters.

9. Rosemary Horne (1983). The distribution of Penguin breeding colonies on the Australian Antarctic Territory, Heard Island, the McDonald Islands, and Macquarie Island.

10. David O'Sullivan (1983). A guide to the Pelagic Nemerteans of the Southern Ocean and adjacent waters.

11. John M. Kirkwood (1983). A guide to the Decapoda of the Southern Ocean.

12. John M. Kirkwood (1983). A guide to the Mysidacea of the Southern Ocean.

13. T.H. Jacka (1983). A computer data base for Antarctic sea ice extent.

14. Gary Burns (1983). The variation of Southern Hemisphere atmospheric vorticity around interplanetary magnetic field sector crossings.

15. Suzanne E. Stallman (1983). Gazetteer of the Australian Antarctic Territory.

16. Peter Keage (1984). Resource potential of the Australian Antarctic Territory.

17. Damien Jones (1983). Snow stratigraphy observations in the katabatic wind region of eastern Wilkes Land, Antarctica.

18. G.R. Copson (1984). An annotated atlas of the vascular flora of Macquarie Island.

19. J.S. Boyd (1983). Invariant geomagnetic co-ordinates for Epoch 1977.25.

ISBN: 0 642 87733 5